TÉCNICO LISBOA

Voltage Distribution Characterization of CIGS Solar Cells Utilizing Luminescence Imaging Method

Rani Andhini Putri

Thesis to obtain the Master of Science Degree in

Energy Engineering and Management

Supervisors: Prof. Luís Filipe Moreira Mendes

Eng. Nicolaas Jacobus Bakker

Examination Committee:

Chairperson: Prof. Duarte de Mesquita e Sousa

Supervisor: Prof. Luís Filipe Moreira Mendes

Member of the Committee: Prof. Jorge Manuel Ferreira Morgado

December 2016

Acknowledgments

I would like to thank everyone that has helped and supporting me all the way and made this thesis possible.

My family: thank you so much for all your support and prayers throughout my journey. I cannot thank you enough. I love you all.

My supervisor at ECN, Klaas Bakker: thank you for all the valuable experience and knowledge you have given me.

My supervisor at IST, Prof. Mendes: thank you for your guidance in completing this thesis.

To all of my lovely coworkers who made the work less stressful and enjoyable: may we meet again one day and play volleyball again (maybe in Indonesia, where it is sunny every day). RM FTW!

"Welcome to the real world. It sucks. You're gonna love it!"

Abstract

Defects in solar cells, such as series resistance or shunt resistance, can limit the efficiencies of solar cells. In order to improve energy production and energy efficiency in solar cells, luminescence imaging method is introduced. The luminescence imaging method is usually performed for quality control to help spotting local defects in solar cells. Luminescence is derived from the radiative recombination of electron and holes. This method is a non-destructive, fast, and versatile imaging method for spatially resolved solar cell and material characterization. There are two variants of luminescence imaging, which are photoluminescence (PL) and electroluminescence (EL). Since thin film cells are getting more attention in photovoltaic area, this thesis is focused on the characterization of $Cu(In,Ga)Se_2$ solar cells. CIGS solar cells emit radiation that is captured by a camera while operates at forward electrical bias, a method known as electroluminescence (EL). Through EL images, voltage distribution can be obtained. In this thesis, Haunschild's method of voltage-mapping is used, where two EL images were taken at different voltages to map the voltage distribution of the cell. Although Haunschild's method has been practiced on silicon solar cells, the aim of this thesis is to transfer the method used in Silicon solar cell to thin films. The measurements were carried out on a small cell, which later will be upscaled to a larger cell. The method proved to provide good results for cells up to $3cm^2$ but it has to be improved to allow characterization of cell with dimension above $5cm^2$.

Keywords: Solar cell, Thin film, CIGS, Photoluminescence, Electroluminescence

Abstrato

Os defeitos de fabrico das células fotovoltaicas reduzem a sua eficiência traduzindo-se em resistências parasitas. A sua caracterização com técnicas de imagem de luminescência é um meio de verificar a existência de defeitos e é utilizada na indústria para efetuar o seu controlo de qualidade. A luminescência decorre da recombinação de eletrões e lacunas com a emissão de fotões. É um método não destrutivo rápido e versátil de obter uma caracterização espacial das células. Existem duas variantes de imagem por luminescência, a fotoluminescência (FL) e a eletroluminescência (EL). Dado o cada vez maior interesse nas células fotovoltaicas de filme fino, o trabalho apresentado nesta dissertação está direcionado na caracterização de células de $Cu(In,Ga)Se_2$ (CIGS). O método principal utilizado para caracterizar as CIGS foi o de imagem de eletroluminescência obtida a partir da aplicação de uma tensão direta que gera uma corrente elétrica, sendo a imagem produzida pela recombinação de carga que ocorre na célula, a eletroluminescência. As imagens de EL permitem um mapeamento das tensões na célula através do método de Haunschild. Tendo este método sido aplicado anteriormente a células de silício, o objetivo do trabalho foi o de estudar a exequibilidade de estender a sua utilização às CIGS, tendo-se obtido bons resultados em células com dimensões até $3cm^2$ e identificado a necessidade de melhorar o método no caso de se pretender caracterizar células de dimensões acima de $5cm^2$.

Palavras Chave: Célula Solar, CIGS, Fotoluminescência, Eletroluminescência

Table of Contents

List of Abbreviations

c-Si	Crystalline Silicon
CB	Conduction Band
CdS	Cadmium Sulfide
CdTe	Cadmium Telluride
CIGS	Copper Indium Gallium Selenide
EL	Electroluminescence
f/14 and f/16	Fully Open and Fully Closed Aperture
I-ZnO	Intrinsic Zinc Oxide
PL	Photoluminescence
PV	Photovoltaic
Si-CCD	Silicon Charge-Couple Device
SLG	Soda-Lime Glass
SNR	Signal-to-Noise Ratio
TCO	Transparent Conductive Oxide
VB	Valence Band
ZnO-Al	Aluminum doped-Zinc Oxide

List of Variables

E	Energy of Photon [eV]
E_g	Band gap Energy [eV]
Ci	Calibration Constant per Pixel
$Qe(E)$	External Quantum Efficiency
R_s	Series Resistance [Ω]
$Vappl$	Applied Voltage [V]
Vi	Local Voltage per Pixel [V]

List of Figures

List of Tables

1.0 Introduction

Nowadays, we use energy to do anything in our daily lives and we all depend on it. Many environmentalists believe that the biggest challenge for human kind is tackling the energy problem, which mainly circles around the climate change [16]. The first challenge is the fast growth of energy demand and supply. Global demand for energy is rapidly increasing, arising from population and economic growth. The more people we have in this world, the more energy we need. This energy need has taken a toll on our environmental systems, where unsustainable practices have dominated, since the main energy source we use today is heavily dependent on fossil fuels. The notorious fossil fuels are known to be unsustainable and remain a threat to the world, because they deteriorate the environment [17]. Energy from fossil resources contains significant amounts of carbon (which is dangerous for the environment) that are normally released during combustion. The report of U.S. Energy Information Administration on International Energy Outlook 2016 studies projects that the world's energy-related carbon-dioxide (CO2) emissions will rise from 32.2 billion metric tons in 2012 to 35.6 billion metric tons in 2020, and to 43.2 billion metric tons in 2040 (reference case of 35% over the projection period) [18]. Therefore, the upsurge of energy demand leads to the rise of fossil fuels that will continue to contribute the rise of CO2, which has been proven to be hazardous to the environment [17].

Energy-related CO_2 emissions are the majority of global GHG emissions that causes climate change. This is the second challenge in energy sector. We can decrease the GHG by lowering the CO_2 emission from switching energy generation from fossil fuels to renewables [18]. Due to this reason, there is an increasing pressure from countries and international organizations towards a clean and diversified energy mix. Within the context of reduction greenhouse gases, renewable energies are developed, not as an alternative, but a solution to the energy question. Renewable energies, such as, solar, wind, hydro-power, biomass, etc are currently showing a tremendous trend in energy sector. References [19] give a brief discussion about different renewable energy technologies. Currently renewable energy continues its rapid growth in both capacity and energy produced. Solar photovoltaics (PV) and wind are the most dynamic markets, and hydropower continues to provide the majority of renewable power capacity and generation. In this thesis, we will focus on solar PV technology.

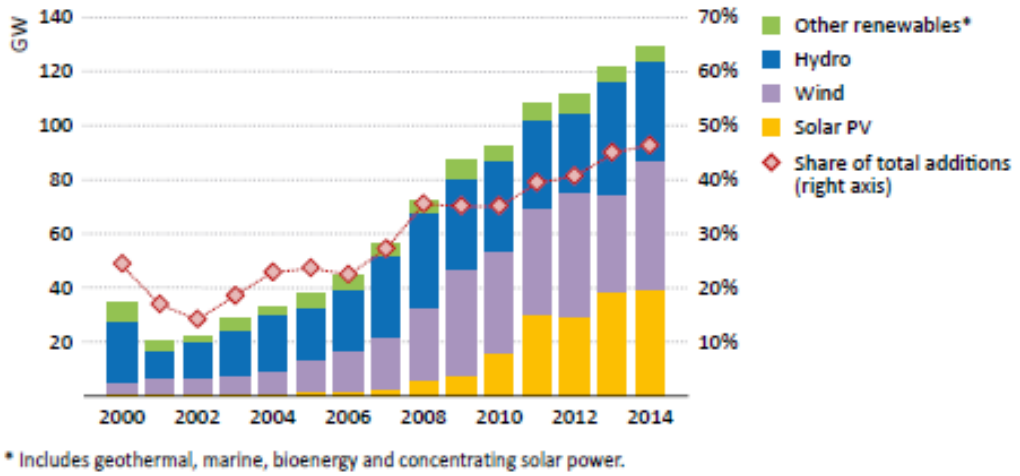

Figure 1.1: Global Renewables-based power capacity additions by type and share of total capacity additions [1]

Between 2006 and 2011, the global PV capacity increased dramatically by an average of 58% annually, the fastest growth of all renewable technologies [20]. Thus, solar energy will continue to contribute as an important part to meet the world energy needs. Fig. 1.1 demonstrates the deployment of renewable energies that has been increasing considerably in recent years. Governmental policies, increase in energy demand, volatility of fossil fuel prices and the declining costs of these technologies have stimulated the continuing increase in the use of renewable energies [17].

Currently in PV sector, crystalline silicon (c-Si) solar cells holds 86% of the market share and dominates in PV sales, while thin-film solar technologies have more or less of 14% [21]. But in the last few years, most new development has been focusing on thin-film PV technologies and the thin film's share of the market has risen steadily. Though, the overall performance of thin film PV technologies are not as efficient as crystalline silicon modules, thin film photovoltaic is an emerging research field due to technological progress and the tremendous growth of the photovoltaic industry in recent years [20]. It can be seen from Fig. 1.2 that the slow growth of crystalline silicon solar cell has led to improvements in other types of solar cells. In addition, thin film PV has also other advantages over crystalline silicon; perhaps most importantly, thin-film solar is much less expensive to produce. Many thin-film panels are produced from amorphous silicon. These solar cells require much less high-grade silicon than it takes to produce crystalline silicon panels. Thin-film solar cells can also be made from other semiconductor materials, including cadmium telluride and copper indium gallium (di)selenide (CIGS) [22].

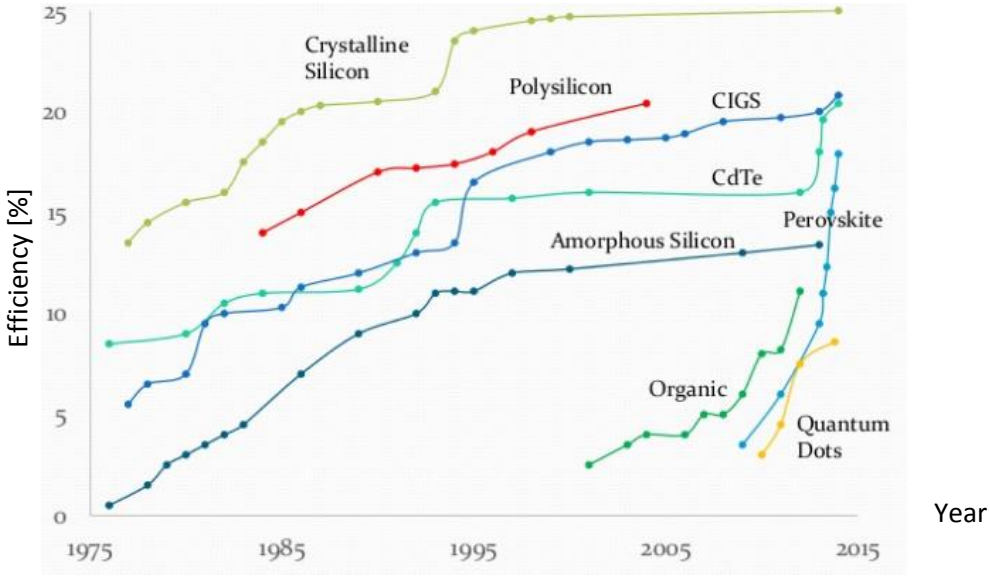

Figure 1.2: The growth of different kinds of solar cell over the years [2]

The future of thin film looks very encouraging. Major improvements in efficiency, stability, and cost are continuously being made and industries are preparing for large-scale production in some of these technologies. If the present trend continues, thin-film solar cells will certainly meet the challenge of the future as the most desirable alternative to the conventional source of power generation [23].

1.1 PV Characterization Technology

As the PV technology is gaining more popularity and its technical aspects are improving fast, the research of a stable and high efficient solar cell is growing rapidly, meaning, researchers are eager in further development of a high efficiency and stable solar cell. Luminescence imaging of solar cells has been introduced recently, and it is a vital technique for quality control of the crystallization process to find defects, which limits the efficiencies of solar cells [24]. The advantage of luminescence imaging method is to visualize and detects defects in solar cells that can affect the efficiency (see Appendix for electrical model of a solar cell). Defects such as shunts and series resistance can be seen on luminescence image in example Fig. 1.3.

Luminescence imaging has recently been demonstrated to be fast experimental techniques that allow measurement of the spatial distribution of the diffusion length in silicon solar cells and of the minority carrier lifetime in large area silicon wafers [25]. Uchida (1963) introduced luminescence imaging by using an infrared-sensitive image converter tube as a detector. Years later in 2005, Fuyuki et al. brought luminescence imaging to the attention of the solar energy area by demonstrating that the electroluminescence emission of silicon solar cells is directly detectable with commercially available silicon charge-couple device (CCD) cameras without the need of an additional infrared image converter [25]. Then in 2006, Trupke at al. introduced optical excitation instead of using electricity, which is called photoluminescence. Within the following years, luminescence imaging went through an

incredibly fast process of improvement and became a versatile characterization technique used in research and industrial environments for the analysis of crystalline silicon wafers and solar cells. [26]

Another advantage of these techniques is that data acquisition times for high-resolution luminescence images are typically on the order of only seconds. Inspection of solar panels during production can improve the quality, lifetime and energy conversion efficiency. When inspection takes place from the earliest moments in production, it helps pick out the downgraded solar cell material before it can get added value through later stages of manufacturing or cause machine downtime from parts broken due to defects. It is, therefore, a huge advantage in utilizing these methods in the fabrication process of solar cells, even modules, in order to achieve high efficiency. [26]

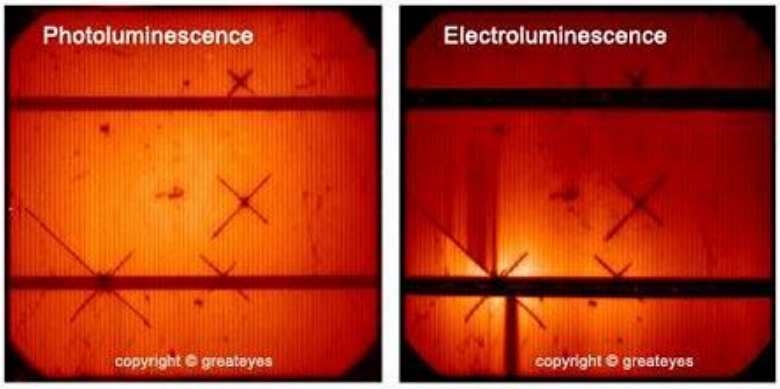

Figure 1.3: Example of defects through photoluminescence and electroluminescence images [3]

1.2 Objective of thesis

The objective of this thesis is to contribute to the progress of the thin film technology through the use of new development characterization technique. Using luminescence imaging method, this thesis aims to extend the study of voltage-mapping method that has been used for crystalline silicon to thin film solar cells, especially CIGS. Numerous studies and experiments have been carried out for silicon solar cells, while there have been limited number of research regarding spatially resolved electroluminescence (EL) and photoluminescence (PL) of thin films [8]. The conversion of these luminescence images into absolute quantities is the main area of research of this thesis, as well as to have a better understanding of the abilities and limitations of the Greateyes system (a device that performs luminescence imaging) that ECN purchased.

Inhomogeneous radiance of solar cells that may be caused by defects, such as series resistance or shunts can be seen through the use of luminescence imaging. In order to have an understanding of the series resistance, a voltage-mapping is necessary. Therefore, the ultimate main goal of this thesis is devoted to the characterization of voltage distribution in solar cells through EL procedure. Hence, this thesis will strongly emphasize on EL rather than PL. Thesis objectives are met by the development of interpreting luminescence images in terms of local voltage, which will be explained further in Chapter 4.1.

1.3 Thesis Placement

The internship has been performed at Energy Research Centre of the Netherlands (ECN), within the thin film projects. ECN is the largest energy research institute in the Netherlands and have been developing new technology and conducts pioneering research in various ways into innovative solutions to facilitate the transition to sustainable energy management. With around 500 members of staff, ECN is active in projects both at domestically and abroad, in joint efforts with the industry, government authorities and research institutes. As part of its work on Sustainable Energy, ECN integrates the Solliance consortium, a partnership of R&D organization from the Netherlands, Belgium and Germany, working on thin film photovoltaics. Solliance works with and for the industry to answer short-term needs and lead promising lines of mid and long-term research. Its main themes are Copper Indium Gallium Selenide (CIGS) and Organic/Perovskite PV, for which Solliance is building the baselines to comply with the industry's most pressing questions. Solliance's research covers the entire field, from fundamentals of materials science to high-end technologies that bring large scale production at low cost in reach. State of the art laboratories and pilot production lines are jointly used for dedicated research programs in close cooperation with the solar business community. Working together with ECN/Solliance, the project goal is to study and analyze the behavior of thin film PV by utilizing luminescence imaging methods.

Inspection of solar panels during production improves the quality, lifetime and energy conversion efficiency. When inspection takes place from the earliest moments in production, it helps pick out the downgraded silicon material before it can obtain added value through later stages of manufacturing or cause machine downtime from parts broken due to defects.

1.4 Thesis Structure

The specific thesis structure is outlined as follows.

Chapter 2 explains the physical concepts, which are needed to understand the work, results and discussions in this thesis. The principle of semiconductor is discussed and the reciprocity theorem is introduced, which explains the relation between the external quantum efficiency of a solar cell and luminescence image resulting from the radiative recombination process. Since this work is mainly focused on thin film technology, $Cu(In,Ga)Se_2$ (CIGS) and its device structures are explained. This chapter also explains the basic principle of luminescence imaging method, which includes the explanation of both PL and EL.

Chapter 3 introduces the experimental setup. Since this work mainly focuses on the analysis of spatially resolved electroluminescence image, the setup is described in detail. It will also explain how reliable the system is for each time luminescence method is performed.

Chapter 4 concentrates on the complete procedure of the methodology. The relationship between voltage and luminescence signal is introduced in this chapter, as well as the measurements

techniques applied in this work. In this chapter, the methodology and analysis of voltage mapping utilizing luminescence method will be explained in detail.

Finally, **Chapter 5** is the conclusion, discussion and future work that can be taken from the experiments.

2.0 Basic Theory

2.1 Semiconductor basic principle

Semiconductors are the basis of a solar cell and have conductivity between that of a metal and an insulator. The electrons in a semiconductor are bounded more strongly than in a metal, but under a certain conditions, e.g. higher temperature, they can be free from their atoms, leaving a positive charge behind (hole). The difference between different materials is illustrated in Fig. 2.1.

Semiconductors have two different bands: the *Valence Band* (VB), a lower electronic band where the electrons are bound to the atoms in the lattice; and the *Conduction Band* (CB), upper electronic band where electrons are free and can contribute to conduction. The band gap E_g is a forbidden region between these two bands and it represents the minimum energy required to excite an electron from the bound state to the free state. Both the electrons in the CB and the holes in the VB contribute to the electrical conduction. At absolute zero (0 K), all energy levels below the so-called Fermi level E_F. As temperature rises, more electrons are excited and can move above the Fermi level to the CB, where they can be used for electric current. [27]

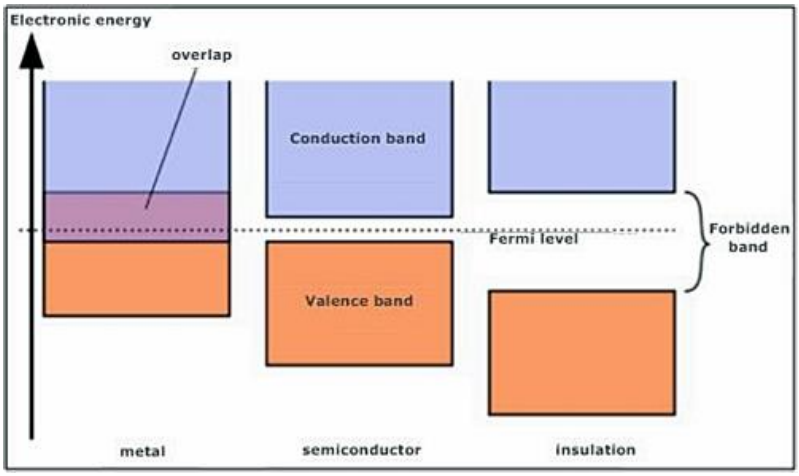

Figure 2.1: Electronic band structure for a metal, a semiconductor and an insulator material [4]

2.2 P-N Junction

Adding impurities to a semiconductor material is a way to increase the carrier concentration. A *p-type* semiconductor material is formed with an increased concentration of positive carriers, while an *n*-type semiconductor is created when electrons are dominant. If these two semiconductor materials are joined together they behave in a very different way and this is called a *P-N junction.* When they first joined together, a very large carrier density gradient exists between both sides of the P-N junction. The result is some of the free electrons from the donor impurity atoms begin to migrate across this newly formed junction to fill up the holes in the P-type material producing negative ions. As a result, the charge density of the P-type along the junction is filled with negatively charged ions and the charge

density of the N-type becomes positive. This charge transfer of electrons and holes across the P-N junction is known as *diffusion.* This process continues back and forth until the number of electrons that have crossed the junction have a large enough electrical charge to repel or prevent any more charge carriers from crossing over the junction [28]. The P-N junction illustration can be seen in Fig. 2.2.

In a doped material, the type of carrier with the highest concentration is called the *majority carrier*, while the lower concentration carrier is called the *minority carrier.* Without illumination and doping, electrons and holes are in equilibrium and an intrinsic charge carrier concentration n_i as a function of temperature is expressed as,

$$n_i = N_C N_V \exp(\frac{-E_g}{kT}) \tag{1}$$

where N_C and N_V are densities of states, E_g is the band gap, k is the Boltzmann constant, and T is the temperature. At a given temperature and illumination, the band gap, $E_g = E_C - E_V$ is constant for a given material [29].

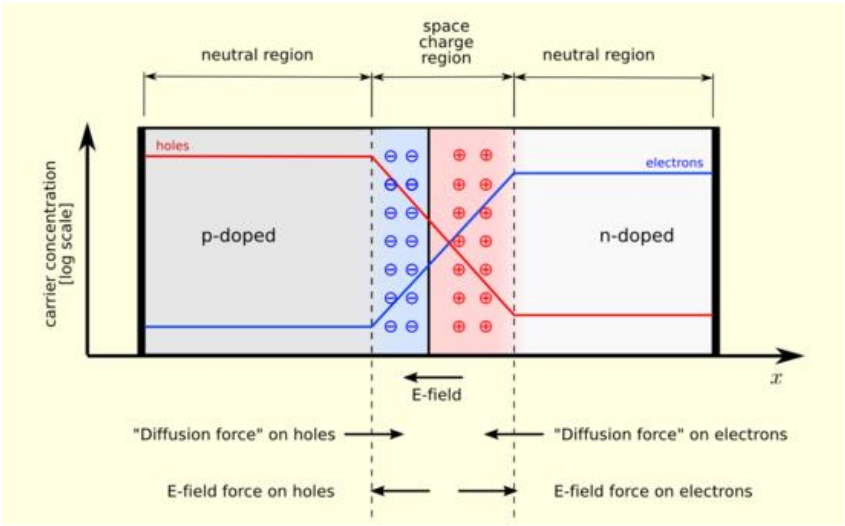

Figure 2.2: P-N junction [30]

2.3 Direct and Indirect Band Gap

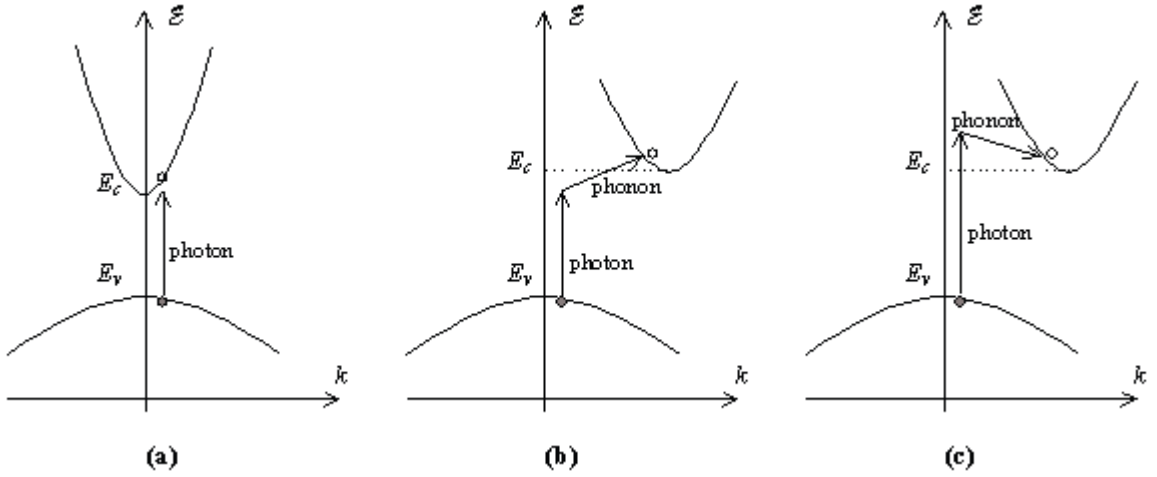

Figure 2.3: $\varepsilon - k$ Band gap diagram [6]

As stated before, the band gap represents the minimum energy difference between the top of the valence band and the bottom of the conduction band, however, the top of the VB and the bottom of the CB are not generally at the same value of the electron momentum. The $\varepsilon - k$ diagram in Fig. 2.3 displays the characteristics of a particular semiconductor material. It shows the relationship between the energy and momentum of available quantum mechanical states for electrons in the material. The direct band gap semiconductor, which has a vertically aligned conduction and valence band, is shown in Fig. 2.3 (a). Absorption of a photon is obtained if an empty state in the CB is available, which the energy and momentum equals that of an electron in the VB plus that of the incident photon. The electron therefore makes an almost vertical transition on the $\varepsilon - k$ diagram. Meanwhile, for an indirect band gap semiconductor, the CB is not vertically aligned to the VB, as shown in Fig 2.3 (b) and (c). Therefore a simple interaction of an incident photon with an electron in the VB will not provide the correct energy that corresponds to the empty state in the CB. Therefore, absorption of light requires the help of another particle, namely a photon. Since a phonon has a relatively low velocity close to the speed of sound in the material, it has a small energy compared to a photon. Conservation of energy can therefore be obtained in the absorption process if a phonon is created or an existing phonon participates. Process (b) shows the absorption of a photon aided by the simultaneous absorption of a phonon, where the minimum photon energy is slightly below the band gap energy. Meanwhile, process (c) illustrates the absorption of a photon resulting in the emission of a phonon, where the photon energy needs to be slightly above the band gap energy. Therefore, it is evident that absorption is much stronger in a direct band gap semiconductor [6].

Light absorption and emission in a semiconductor is known to be heavily dependent on the band structure of the semiconductor. Direct band gap semiconductors have a stronger absorption of light as characterized by a larger *absorption coefficient*, which determines how far into a material light of a particular wavelength can penetrate before it is absorbed. While indirect band gap semiconductors are known to have a smaller absorption coefficient. The demonstration of absorption and emission of photon is illustrated in Fig. 2.4

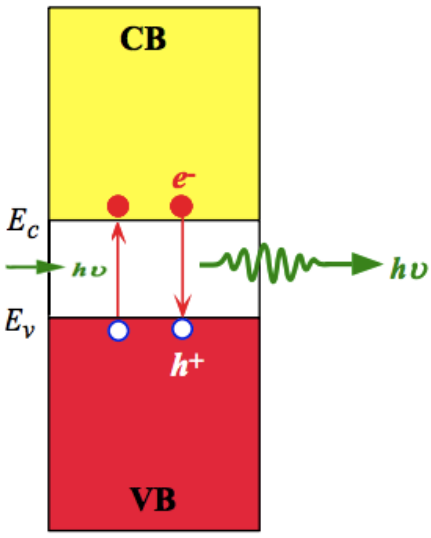

Figure 2.4: Demonstration of absorption and emission of photon [5]

2.4 Absorption Coefficients

Solar cells are *opto-electronic* devices, meaning they convert energy from incoming photons into electrical energy. The goal for any solar cell is to absorb light as efficiently as possible, thus, solar cells absorbers should be nontransparent for photons with energy $E > Eg$. Electron-hole pairs are created when photons with energies exceeding the band gap energy of the semiconductor are absorbed. These electrons and holes created by the absorption process are called excess carriers. When the excess carriers arise, they can dominate in the conduction process in the semiconductor material. This means, electrons can be excited to the conductions band either by light absorption or separation of charge carriers, which is achieved by applying a forward bias voltage across a p-n junction diode.

When a photon enters a device and if the photons contain energy larger than the band gap, there will be some predictable amount of absorption, determined by the properties of the material. Furthermore, the extra energy will be released as heat. If the incident photon has energy equal to the band gap, it can be absorbed in the semiconductor material and excite the electron to the CB. However, if the energy of the photon is lower than the energy of the band gap, it cannot be absorbed.

Different semiconductor materials have different absorption coefficients. Materials with higher absorption coefficients can absorb more photons, and knowing the coefficients of materials may help engineers in determining which material to use in their solar cell designs. The equation for the coefficients differ in terms of the band gap type, which is expressed as,

$$\alpha_{dir} \propto \sqrt{(hv - E_g - E_p)} \quad (2)$$

$$\alpha_{ind} \propto (hv - E_g \pm E_p)^2 \quad (3)$$

With α as absorption coefficient, hv is the photon energy, E_p is the energy of phonon that is either absorbed or emitted, and E_g is the band gap energy. Equation (2) is the absorption coefficient for

direct semiconductor, while equation (3) demonstrates the absorption coefficient for indirect semiconductor [31]. The dependency of the absorption coefficient to photon energy is plotted in Fig. 2.5.

Fig. 2.5 compares the absorption coefficient of different semiconductors. The blue curve represents silicon (c-Si), which is an indirect band gap, and the red curve represents a direct semiconductor (in this case, it was performed on $CuInSe_2$). From Fig. 2.5, it clearly depicts that direct band gap exhibits much higher absorption, making direct band gap material to be attractive [7].

Direct semiconductor materials have larger absorption coefficient α close to their band-gap energy, meaning that they have a stronger light absorption. While the indirect semiconductors have longer absorption length, this means that indirect semiconductors, i.e. c-Si wafers, are usually thick; if it was much thinner, much of the light would simply pass through. Cu(In,Ga)Se2 (CIGS) is a direct semiconductor. Furthermore, thin-film solar cells are made of direct band gap materials (such as CdTe and CIGS), which absorb the light in a much thinner region, and consequently can be made with a very thin active layer (1-3 μm) [10].

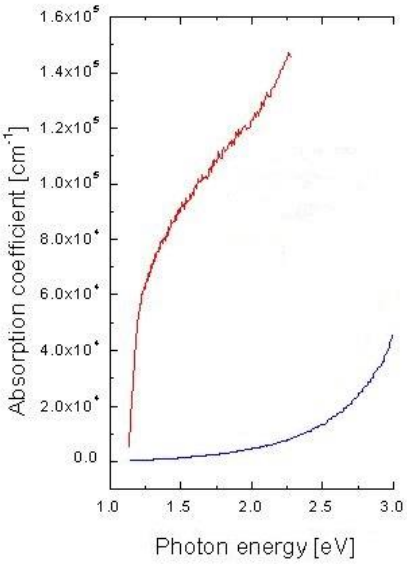

Figure 2.5: Absorption coefficient graph [7]

2.5 Recombination Process

When a semiconductor is disturbed from the equilibrium state, the carriers change from their equilibrium values. When there is a surplus of carriers, recombination drives back toward equilibrium [32]. The electron and hole pairs are called excess carriers since they are out of balance with their surroundings, but they will eventually recombine. While the excess carriers exist in their respective bands, however, they are free to contribute to the conductivity of the material. Recombination is the reverse process of a generation. It is a process in which an electron and a hole recombine, and the energy is released as either a photon, a phonon, or both to return to its equilibrium state [29].

2.5.1 Types of recombination

Any electron that exists in the conduction band is in a meta-stable state and will eventually stabilize to a lower energy position in the valence band. When this happens, the electron must move into an empty valence band state. Thus, when the electron stabilizes back down into the valence band, it also removes a hole. As previously mentioned, this process is called recombination. There are three types of recombination that can be seen in Fig. 2.6: Auger recombination and Shockley-Read-Hall recombination producing phonons, and radiative recombination that produces photons.

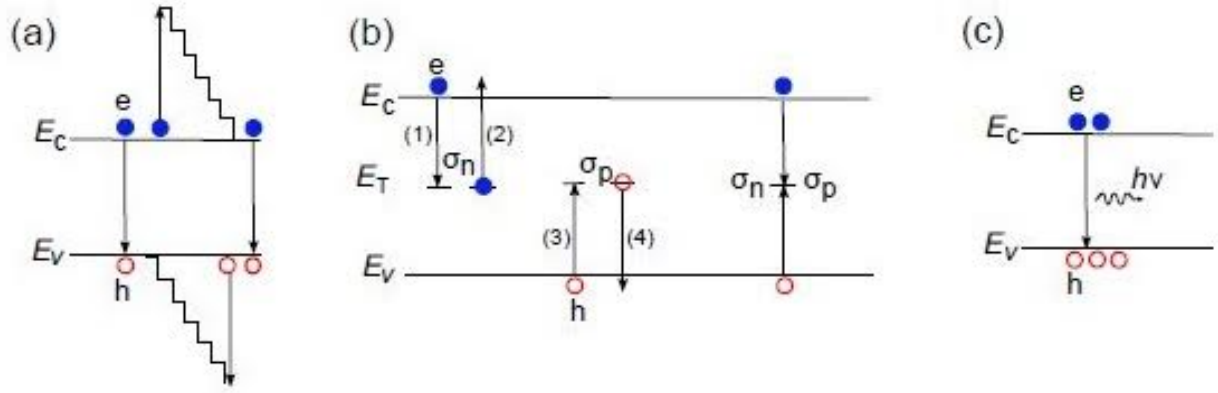

Figure 2.6: (a) Auger Recombination, (b) Shockley-Read-Hall, (c) Band-to-Band Recombination [8]

Auger Recombination. It is a recombination mechanism that involves three carriers. An electron and a hole recombine, but instead of emitting the energy as heat or as a photon, the energy is given to a third carrier (an electron in the conduction band). This electron will eventually thermalizes back down and loses its energy as phonons when it is going back to the conduction band edge.

Shockley-Read-Hall. This recombination process is associated with defects in the lattice. The defects create new energy levels within the band gap, where electrons and holes can recombine with lower energy associated. In this process, electrons in the CB are captured by impurities with energy states within the forbidden region, and from there they relax into a lower energy state, or into the valence band. The energy released during each transition is emitted as phonons. The rate at which a carrier moves into the energy level in the forbidden region depends on the distance of the introduced energy level from either of the band edges. If close to the band edges, e.g. the conduction band, recombination is less probable as the electron is likely to be re-emitted to the conduction band edge rather than recombine with a hole, which moves into the same energy state from the valence band. For this reason, energy levels near mid-gap are very effective for recombination [33].

Band-to-Band Recombination. This type of recombination is an important recombination process since it is the fundamental process for luminescence. Band-to-band recombination is also known as a radiative recombination process. Radiative recombination occurs when an electron n in the CB recombines with a hole p in the VB, and thereby, emits a photon γ. Radiative recombination happens

when all or part of the energy released as a result of the recombination of an electron in the conduction band is emitted as a photon. The rate of photons generated due to radiative recombination is given by:

$$G_{photon} = R_{electron} = R_{hole} = B_T n_0 p_0 \quad (4)$$

Where $R_{\frac{electron}{hole}}$ are the recombination rates of electrons and holes respectively, B_T is the coefficient for radiative recombination (which depends on the temperature), and n_0 and p_0 are the concentrations of electrons and holes, respectively [29]. In an ideal direct band gap semiconductor like CIGS, the radiative recombination process is usually the predominant process.

In general, the loss mechanism of recombination defines the lifetime of the carriers. If the recombination is high, the lifetime of the carrier is low. In this case, the diffusion length – the average distance carriers can move through before recombining – is shorter.

2.6 Luminescence Imaging

The band-to-band radiative recombination is the basic fundamental of how luminescence procedure works. Luminescence imaging techniques are spatially resolved method where photons emitted by radiative recombination in PV devices are captured by a detector. Spatially resolved luminescence images have been used in PV research for quite some time and the benefit of using this technique as a characterization tool for solar cells have been pointed out previously by various authors [34]. Furthermore, the luminescence signal is directly proportionate to the photons created from radiative recombination. [35] A high-resolution image of the distribution of the luminescence intensity contains information about essential properties of a solar cell, few of them includes:

1. The distribution of the voltage over the surface, from which the distribution of series resistances and shunts may be derived indicating shortcomings of the production process.

2. The distribution of the diffusion length of the minority carriers indicating the quality of the solar cell material.

3. The distribution of the back surface recombination indicating the quality of the surface passivation (which is important to avoid high recombination rates on the surface that may lead to short-circuit currents).

However, in this thesis, luminescence imaging will be used to calculate and identify the voltage distribution across the cell. Furthermore, luminescence imaging is divided into two approaches: Photoluminescence (PL) and Electroluminescence (EL). The image that is captured shows a distribution of luminescence photons emitted from the sample's surface. Both procedures may be used to measure and determine the overall uniformity of a cell well as locate defects, since these factors are disadvantageous for the cell efficiency [36]. Usually, the non-uniformities are a result of

manufacturing process. EL and PL can be vital tools to help in determining the physical causes of non-uniformities that can be seen by abnormalities in luminescence images. The main important key for a high production yield is an efficient inspection tool at the early stage of the production process.

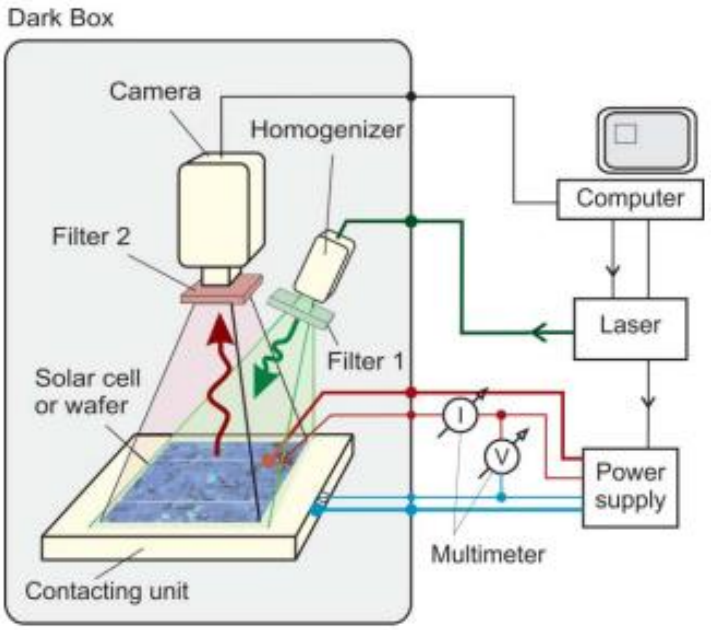

Figure 2.7: Common Setup for EL PL [9]

2.6.1 Photoluminescence

The deviation from the thermal equilibrium can be disturbed by various forms of excitation, such as external voltage injection, an incident electron beam, mechanical stress, or by the absorption of light of sufficient energy [20]. The emission from PL radiation is caused by the transition of electrons from higher occupied electronic states into lower unoccupied states, which recombine with holes. The advantage of PL is the fact that the procedure does not need electrical contacts and can be applied after the absorber deposition prior to the transparent conducting oxide (TCO) deposition and the completion of the cells/modules [37], typically in CIGS solar cell.

A schematic of typical PL and EL setup is shown in Fig. 2.7. The sample is mounted in ambient conditions for fast room-temperature measurements. As an excitation source, any light source of suitable luminance and appropriate wavelength range can be used. PL method requires a homogeneous illumination across the sample to have every part of the solar cell generates uniform electron-hole pairs. Since the excitation source needs to be homogeneous across the cell's surface, in most setups, lasers are used because of its widespread ability. The lasers are directed onto the sample homogeneously. A camera collects the luminescence or the photons emitted by the electron-hole recombination from the sample. Before the lens of the camera, the photons pass a filter,

preventing the detection of unwanted stray lights. With a computer connected to the system, a luminescence image is displayed on the monitor.

2.6.2 Electroluminescence

The working principle behind EL is technically the same, but instead of exciting the sample with a light source, the sample is injected with carriers to create a recombination process, yielding the photon emission. The emission of light is in consequence to the application of a forward voltage bias to a diode, which is the reciprocal action to the standard operation of photovoltaic. Therefore, all important physical processes that influence the photovoltaic performance of a solar cell, such as recombination, resistive, and optical losses, are in a complementary way reflected in the EL of the device [20].

2.6.3 Photon Emission

Luminescence photon is the energy released in the form of light (luminescence) from the recombination of electron and hole. Emission of photons as a result of band-to-band radiative recombination is a common phenomenon observed in a direct band gap semiconductor, such as GaAs, GaN, CIGS, or ZnSe [8]. Fig. 2.8 illustrates the spectrally response PL that was measured on CIGS at ECN (ECN doesn't have spectrally response EL device), with a wavelength peak of 1096nm. A further explanation of spectral response PL is explained in Appendix 4. However, since this thesis focuses on EL, the theory of photon emission in this chapter is based on the radiation of photon through EL process.

The generation of photon through EL procedure is called the reciprocity theorem [38]. For a solar cell, the external quantum efficiency $Q_e(E)$ is an important quantity and a $Q_e(E)$ graph of a CIGS that was manufactured at ECN can be seen from Fig. 2.9. Further explanation of quantum efficiency can also be found in Appendix 3.

As mentioned before, the relationship of external quantum efficiency and homogeneity of the solar cell affect the efficiency of cell. The relationship between the external quantum efficiency $Q_e(E)$ and photon emissions by EL procedure $\boldsymbol{\Phi_{el}}$ is given by the reciprocity theorem (further explanation in Appendix 5), which is defined as,

$$\Phi_{el}(E) = \mathrm{Q}_e(E)\Phi_{bb}(E)[exp\left(\frac{qVi}{kT}\right) - 1] \tag{5}$$

where $\frac{kT}{q}$ is the thermal voltage, Vi is the internal junction voltage, E is the photon energy that depends on the wavelength $E = \frac{hc}{\lambda}$, $Q_e(E)$ is the local external quantum efficiency, and

$$\Phi_{bb}(E) = \frac{2\pi E^2/(h^3c^2)}{\exp\left(\frac{E}{kT}\right) - 1} \tag{6}$$

is the spectral photon density of a black body [8]. The external quantum efficiency $Q_e(E)$ is defined as the ratio of the number of carriers collected by the solar cell to the number of photons of a specific wavelength impinging on the surface of the device,

$$Q_e(E) = \frac{1}{q}\frac{dJ_{sc}}{d\Phi_{\text{in}}(E)} \tag{7}$$

where $d\Phi_{\text{in}}(E)$ is the incident photon flux in the energy interval dE, which leads to dJ_{sc} (short circuit current density).

This reciprocity theorem has also been further extended to the case of PL emission $\Phi_{pl}(\Phi_{exc}, E)$ resulting from the photo-excitation Φ_{exc} by Rau [39]. This generalized reciprocal relation is given by,

$$\Phi_{em}(E) = \Phi_{sc}(E, \Phi_{ex}) + \Phi_{el}(E, V_i) = \Phi_{sc}(E, \Phi_{exc}) + Q_e(E)\Phi_{bb}(E)[\exp\left(\frac{qV_i}{kT}\right) - 1] \tag{8}$$

Equation (8) shows the emission $\Phi_{em}(E)$, as a function of photon energy, is a superposition of the EL emission Φ_{el} stimulated by the junction voltage V_i and the short circuit (sc) emission Φ_{sc} resulting from the photo-excitation Φ_{exc}.

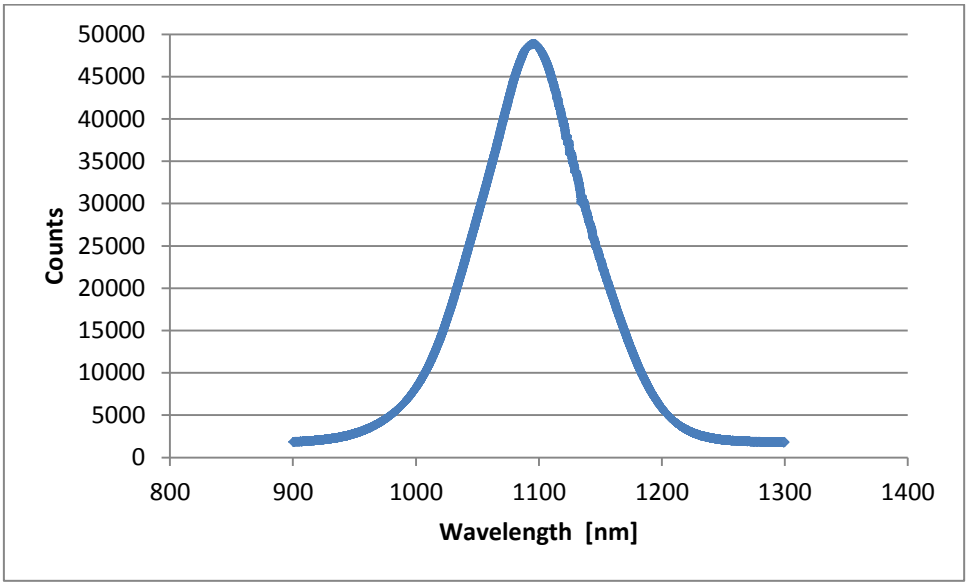

Figure 2.8: CIGS cell spectral response PL measured at ECN

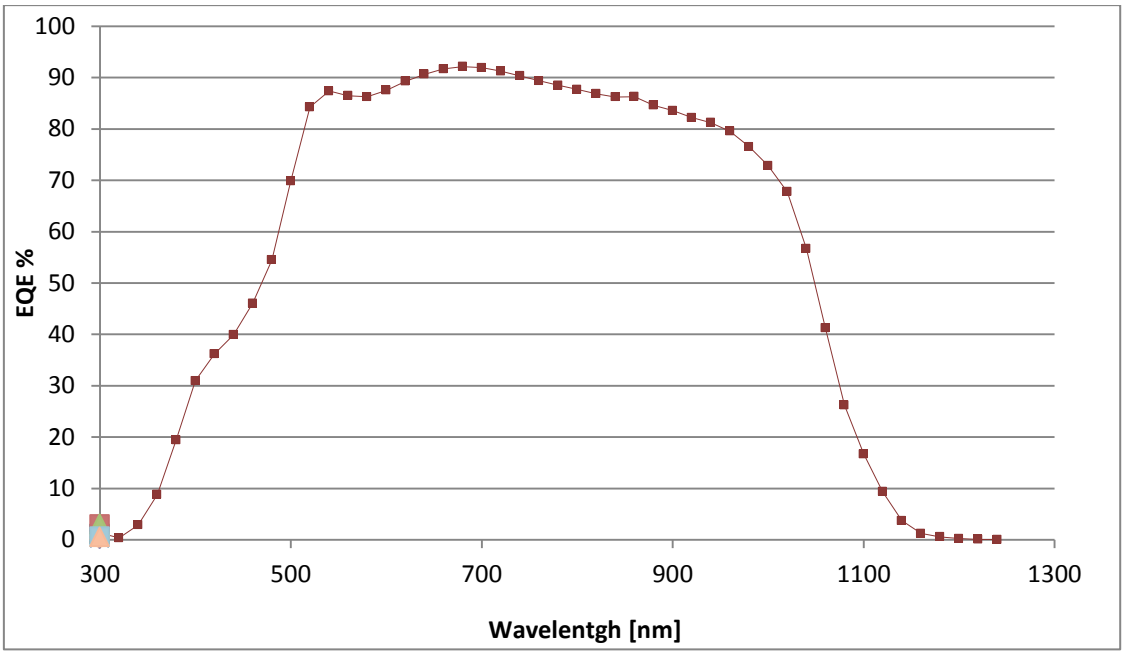

Figure 2.9: External Quantum Efficiency of a CIGS produced at ECN

Furthermore, when detecting the EL emission of a solar cell by a charge coupled device (CCD) camera, the EL signal $S_{cam}(E)$ in each camera pixel is given by,

$$S_{cam}(E) = \int Q_{cam}(E)Q_e(E)\Phi_{bb}(E)dE \exp(qVi/kT) \quad (9)$$

with Q_{cam} being the energy-independent sensitivity of the detecting camera. In equation (5) $\Phi_{bb}(E)Q_{cam}(E)$ is a constant energy-dependent factor for all surface positions of pixel i. Thus, signal variations in the detected intensity emitted from different surface positions originate only from the changes of the external quantum efficiency Q_{el} and of the internal voltage Vi. From these equations, it is evident that the luminescence intensity is dependent on the internal voltage [38].

2.7 CIGS Solar Cell

It has been mentioned several times in previous chapters that CIGS cell is a direct band gap semiconductor that is able to absorb light in thinner region. Solar cells and modules based on the chalcopyrite compound Cu(In,Ga)Se_2 (CIGS) has achieved one of the highest efficiencies among the thin film technologies, with GaAs being the highest of 28.8% [40]. CIGS is one of the cells that is widely researched and developed thin film technology with efficiency currently proven to be up to 21.7% [40]. CIGS is a realistic option for reaching the goal of low-cost, high efficiency power conversion from renewable sources with thickness generally below 2 μm [41]. Before CIGS was discovered, the initial development was only on Copper Indium Diselenide ($CuInSe_2$), later on, scientists revealed that by substituting Galium (Ga) for Indium (In), the bandap increases from about

1.04eV for CIS to about 1.68eV for CGS. Therefore, with only partial substitution of Ga for In can increase in overall efficiency and more ideal bandgap.

A typical CIGS thin film layer consists of six layers:

1. **Glass, Metal Foil, Plastics**

   The glass functions as a substrate to support the thin solar cells. At Solliance, the glass used is soda lime glass (SLG) for about 1-3mm thickness. SLG is used mainly for the reason because it is relatively cheap and contains both sodium and potassium. The purpose of using sodium (Na) is to improve the electronic properties of the absorber [10]. According to Salome et. al, Na increases the free carrier density by at least one order of magnitude and this is associated with a lower number of compensating donors. Na influences the CIGS growth and increased texturing of thin films. Furthermore, the presence of Na in the CIGS layer is beneficial for increasing cell efficiency, but controlling the quantity of incorporated Na into the CIGS during growth is a problem. Reference [42] discuss in detail regarding sodium doping of CIGS solar cells.

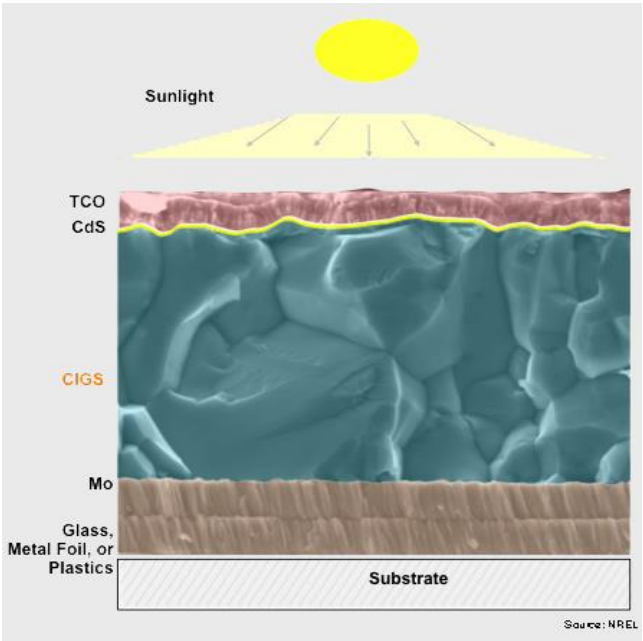

Figure 2.10: CIGS structure [10]

2. **Molybdenum, Mo**

   Molybdenum role is to create an effective electrode for the back contact and to transport the generated holes to the absorber. There is a thin layer of molybdenum selenide to provide a good ohmic contact for the majority carriers. Moreover, this layer shows good conductivity, acceptable adhesion, have reasonably smooth and allow beneficial sodium diffusion that is necessary for the formation of good CIGS absorber. Molybdenum can withstand the temperatures required for CIGS production processes and do not react with the metals in the CIGS absorber (copper, indium and gallium). Mo is commonly deposited by sputtering

technique (a process where the substance are spewed from a solid target material due bombardment of the target by energetic particles. Usually, Mo layer is around 0.3-1μm in thickness. [10]

3. **CIGS layer**

   The absorber, CIGS, acts as the P-type and has a thickness of 1-3μm. Light is absorbed and electron-hole pairs are created. This layer consists of copper indium gallium diselenide, which has a direct bandgap and a high optical absorption coefficient [10]. Used in this thesis, the absorber is deposited by the vacuum co-evaporation.

4. **Cadmium Sulfide, CdS**

   The buffer, CdS, acts as the N-type and added on top of the absorber. CdS serves as a buffer layer because many of its physical properties, e.g. bandgap and refractive index are between those of the ZnO window layer and CIGS absorber layer. The CdS deposition provides a complete covering of the rough CIGS surface and a good passivation of the CIGS/CdS interface [10]. CdS is normally deposited via chemical bath deposition and has a thickness of 50nm.

5. **Transparent Conductive Oxide, TCO**

   The standard sequence of the window layer TCO front electrode in this device consists of 50nm of intrinsic zinc oxide (i-ZnO) and 150nm of aluminum doped (ZnO:Al). i-ZnO is a highly resistive material and it is used to prevent the establishment of shunt paths within the solar cells. The role of the i-ZnO layer in the CIGS device is discussed in Ref. [43], in which the authors discussed that the local series resistance provided by the i-ZnO mitigates the effects of the electrical inhomogeneities that limits the open-circuit voltage of the device. I-ZnO usually deposits by RF sputtering. Meanwhile, the aluminum-doped ZnO (ZnO:Al) n-type semiconductor is transparent and conductive. This layer needs to be transparent to enable light to penetrate through the CIGS absorber layer. It also needs to be conductive to transport the electrons. This layer is deposited by RF sputtering method. [10]

6. **Current Collecting Grid**

   To assist the collection of the produced current, metallic grids are applied on top of the TCO. Current collecting grids can either be thermally evaporated through micro structured shadow masks, made by lithographic methods, or printed. Larger amounts of metal in the grids typically provide better conductivity and, as a result, the efficiency losses due to an increase of the cell dimension are smaller. The efficiency of a metal grid current collector is determined by the conductivity of the metal grid and the distance between the grid lines [44].

3.0 Experimental Setup

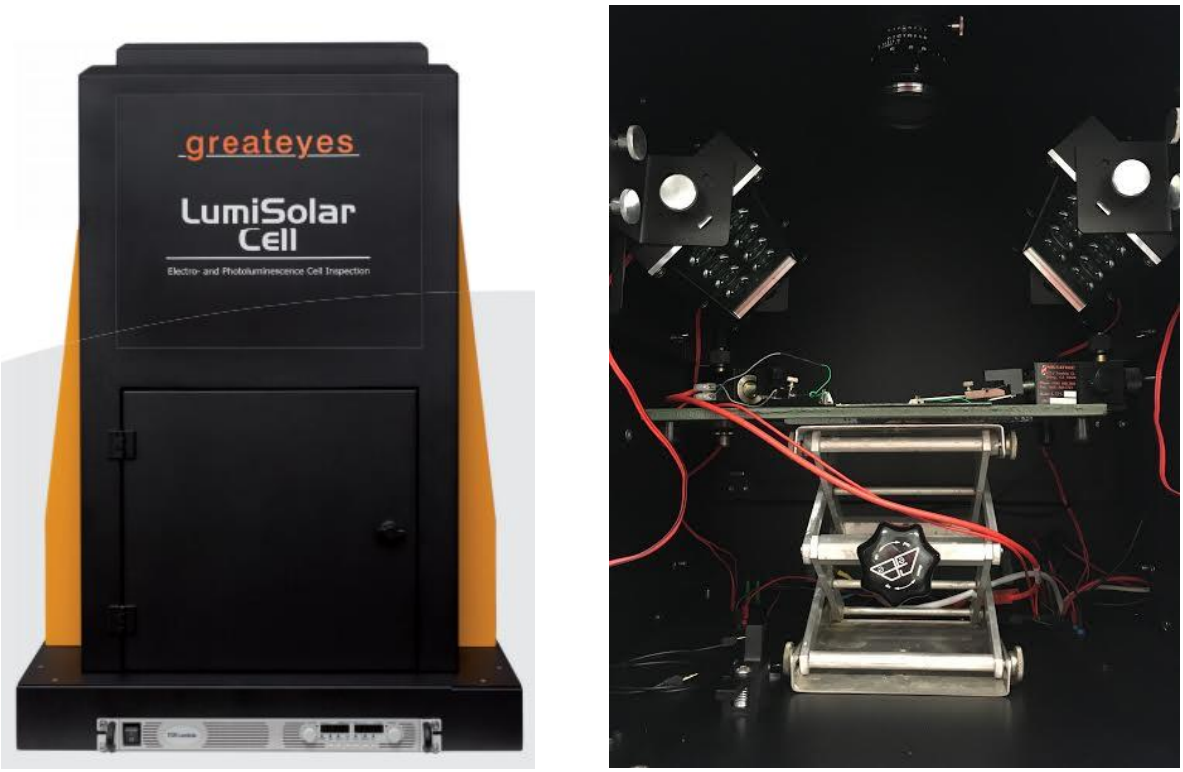

Figure 3.1: The luminescence setup at Solliance [3]

3.1 Introduction to Greateyes system

An EL/PL system can help to optimize solar cells or modules, increase cell efficiency, maintain high quality standards, track problems along the production, increase yield and reduce production cost. Thus, purchasing a device for EL/PL is necessary for ECN. The system that is used in this thesis is Greateyes LumiSolarCell.

The Greateyes LumiSolarCell system utilizes the photoluminescence or alternatively the electro-luminescence procedure to image micro cracks, cell failures and inhomogenities solar cells, which are extremely difficult to detect visually [3]. The equipment enables performing detailed quality control and it was developed for research and industrial inspection. The system consists of a highly sensitive CCD-Camera and an innovative HighPower LED light source, developed and manufactured by Greateyes [3]. Instead of lasers, this setup uses LEDs since they are cheaper and safer, although, more filters are needed to block reflections and stray lights. The system is delivered with a complete enclosure and an optional computer system. The system consists of:

1. **CCD Camera**

   A charge-coupled device (CCD) is a light sensitive integrated circuit that stores and displays the data for an image in such a way that each pixel in the image is converted into an electrical charge [45]. Although the camera has a focusing lens, it is not equipped with a zoom lens; thus, an adjustable board is needed in order to raise the cell height to get a better picture of small cells. The resolution of the image is 1024x1024.

Fig. 3.3 displays the EL spectra of different solar technologies and the external quantum efficiencies of the Si-CCD (Silicon) and InGaAs (Indium Gallium Arsenide) cameras, which was obtained from Jülich Forschungszentrum (Research center in Germany). The spectra that is shown in Fig. 3.3 are normalized to their respective maximum. The external quantum efficiency $Q_{cam}(InGaAs)$ indicates that the low noise InGaAs camera enables the detection of light emitted in a wide spectral range of 800 ≤ λ ≤ 1700nm, conforming to photon energies of around 0.73 ≤ E ≤ 1.4eV. Therefore, InGaAs camera is suitable for EL measurements of all three PV cells. The Si-CCD camera is sensitive in a spectral range of 350 ≤ λ ≤ 1100nm, corresponding to photon energies of around 1.17 ≤ E ≤ 3.5 eV. The EL signals from a-Si:H, c-Si, and CIGS are also detectable with a Si-CCD camera. Si-CCD cameras are more commonly used because they are about a factor of ten cheaper than the InGaAs cameras [8].

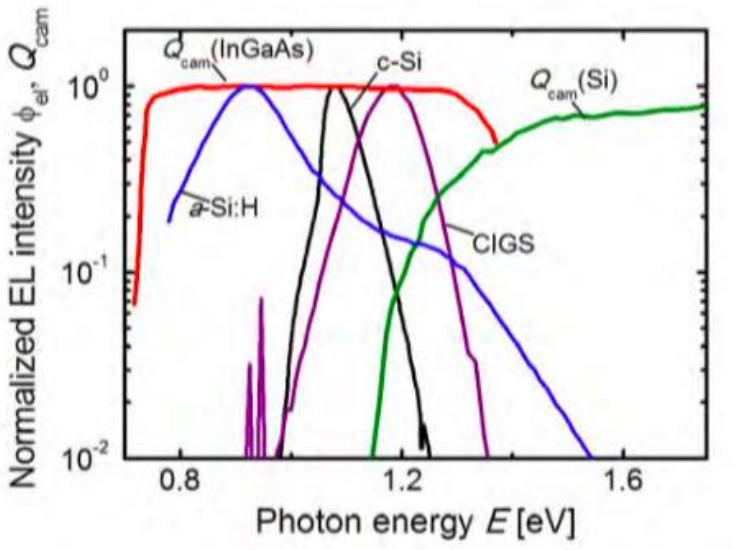

Figure 3.2: Plot of external quantum efficiencies $Q_{cam}(Si)$ and $Q_{cam}(InGaAs)$, and the normalized EL spectra of a crystalline silicon, a-Si:H and a CIGS solar cell [8]

Figure 3.3: Greateyes' silicon camera [3]

2. Light Source

Greateyes system uses LEDs as excitation source and it provides 3 different wavelength LEDs: Green (520-550nm), Blue (460-490nm) and Red (620-645nm). These LEDs are mounted inside the chamber in such a way that the angle of LED arrays can be adjusted for optimum spatial homogeneity. The LEDs are used for PL procedure and they are turned on continuously during the integration period. In addition, there is also a filter just after the LEDs to remove the infrared spectrum tail.

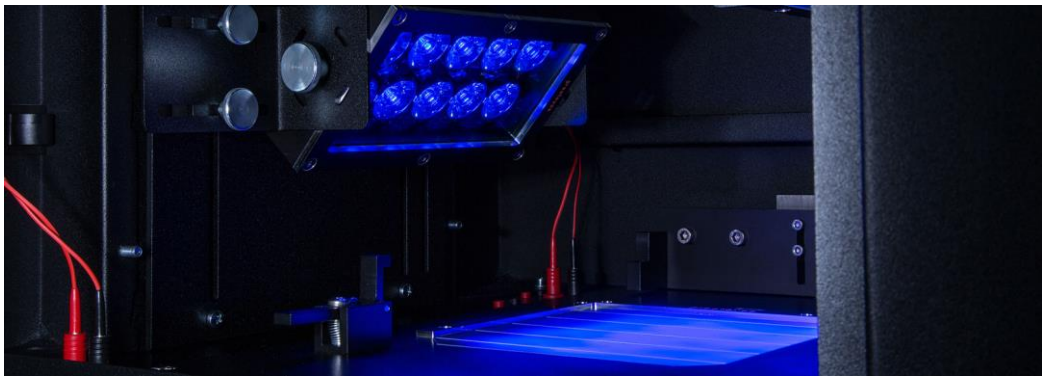

Figure 3.4: Adjustable LEDs [3]

3. Aperture

The aperture of the camera can also be set, ranging from f/1.4 (fully open) to f/16 (fully closed). In this experiment, all the EL measurements were taken at fully open aperture condition, allowing the photons to be captured by the camera in short integration time with high counts as well.

Figure 3.5: Camera mounted on the system [3]

4. Filters

Optical filters in front of the camera are necessary to block non-luminescence light. For PL measurements, the blocking of reflected excitation light is crucial, especially in case of silicon sensor camera. The system's filters are both long pass filters of 750nm and 900nm. The spectrum in Fig. 3.6 illustrates the excitation light sources and the curves of the filters. The Red LED has a peak at approximately 660nm, whereas the green LED's peak is approximately 530nm. The long pass filter (green line) opens after 750nm and it is placed behind the camera lens. While the other filter (purple line) opens after 900nm and it is placed in front of the lens. High pass filter can be removed for higher sensitivity if necessary.

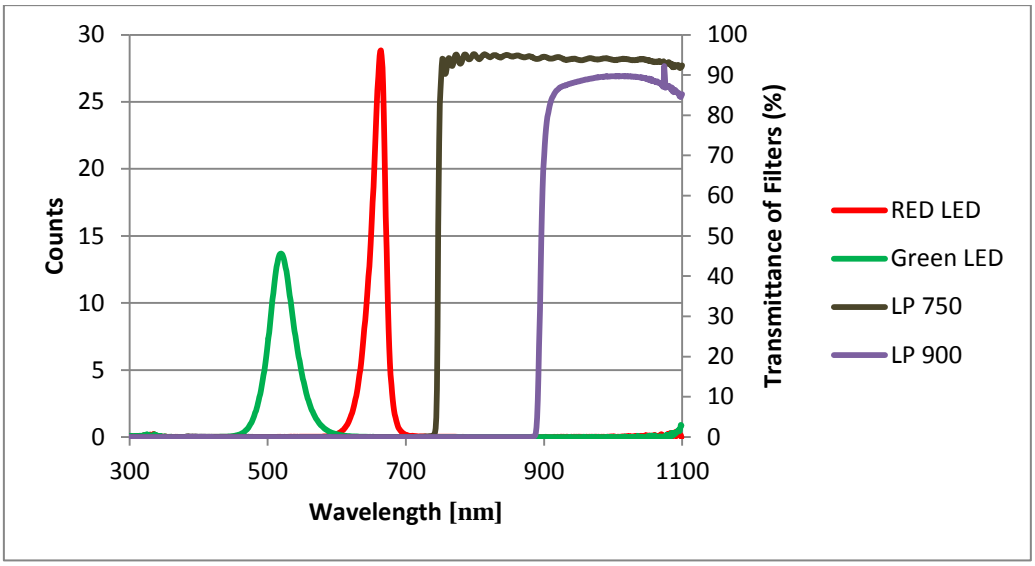

Figure 3.6: Luminescence spectra of LEDs filters measured at ECN

5. TDK Lambda Internal Power Supply

The TDK Lambda internal power supply is controlled by the LumiSolarCell Software. It supplies power to the LEDs and has an adjustable with a maximum current of 4.5A and maximum voltage of 70V.

Figure 3.7: TDK power supply [11]

6. KEPCO External Power Supply

Kepco is used to supply electrical contacts and power to the solar cell and it is used for the electroluminescence procedure. It is a programmable power supply, 0-50V and 1-10A. Both TDK and Kepco are not just to supply power, since it is a 4 quadrant supply, it can be used to dissipate power from the cell.

Figure 3.8: Kepco power supply [12]

7. **Keithley Power Supply**

Keithley power supply is an alternative source for current and voltage injection. While measuring EL using the Kepco, several cells were short circuited, concluding that the Kepco is also a very powerful tool for current injection to use on the small thin film solar cells.

Figure 3.9: Keithley power supply [13]

8. **LumiSolarCell Software**

The LumiSolarCell software controls the camera and visualizes the data sets. The program generates intensity profiles from the 16bit high dynamic range image data. Basic picture manipulation procedures are included in the software. Dimension measurements of artefacts are possible following calibration as well as remote control of power supply and high power LED light source.

In order to get to know more of the system, reproducibility test, accuracy in counts and different time integration assessment are performed. These are vital for quality control assessment and the reliability of the machine.

3.1.1 Reproducibility

To validate how reliable and accurate each time a measurement is done by the Greateyes system, a reproducibility test is carried out. Reproducibility test case is a way to know whether or not the luminescence signal is consistent each time EL image is taken. Several EL measurements were performed and recorded at the same injection current density, with the same camera settings (seen in Fig. 3.10). The cell was injected current from 1.6mA (low power) up to 16mA (high power and Isc). The average counts over the cell were recorded each test. Although the average intensity obtained from these EL images does not show significant deviation, a percentage of deviation was still calculated for each measurement. The percentage deviation was calculated by focusing on the average values only.

$$\%deviation = \left|\frac{maximum - minimum}{(maximum + minimum)/2}\right| * 100\% \quad (10)$$

Table 1: Percentage deviation data

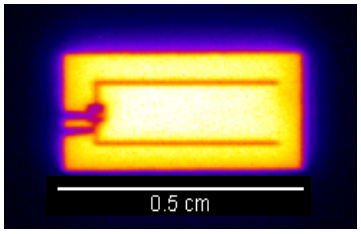

1.6mA 581mV 60s

	Min	Max	Average
1st meas.	4871	51564	40033
2nd meas.	5024	51651	40069
3rd meas.	4923	51651	40237
4th meas.	4878	51862	40334
5th meas.	4863	51526	40164
Average	**4911**	**51630**	**41622**
		%deviation= 0.72%	

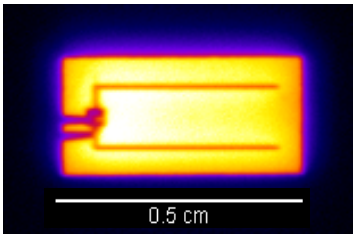

8mA 650mV 8s

	Min	Max	Average
1st meas.	4942	58456	44513
2nd meas.	4858	57828	44005
3rd meas.	4941	57682	43848
4th meas.	4842	57511	43724
5th meas.	4883	57570	43695
Average	**4893**	**57809**	**43957**
		%deviation= 1.86%	

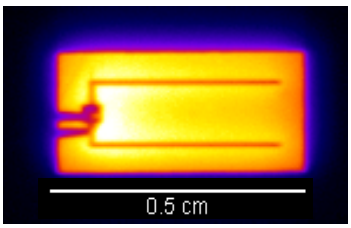

16mA 693mV 150ms

	Min	Max	Average
1st meas.	262	2732	1855
2nd meas.	229	2595	1736
3rd meas.	279	2544	1717
4th meas.	222	2517	1719
5th meas.	248	2530	1715
Average	**248**	**2583**	**1748**
		%deviation= 8%	

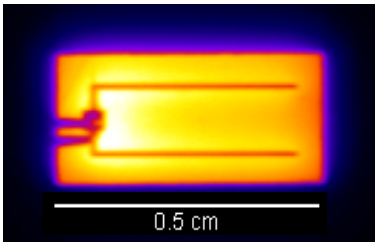

16mA 693mV 500ms

	Min	Max	Average
1st meas.	770	8912	6089
2nd meas.	718	8565	5873
3rd meas.	724	8580	5851
4th meas.	717	8642	5887
5th meas.	679	8606	5880
Average	**722**	**8661**	**5916**
		%deviation= 4%	

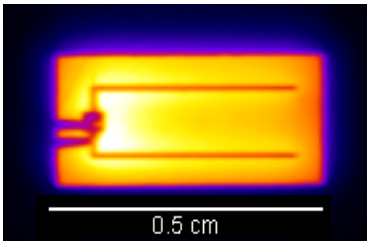

16mA 693mV 1s

	Min	Max	Average
1st meas.	1112	18318	12368
2nd meas.	1112	18111	12334
3rd meas.	1123	18216	12345
4th meas.	1102	18171	12356
5th meas.	1112	18318	12368
Average	**1112**	**18229**	**12354**
		%deviation= 0.275%	

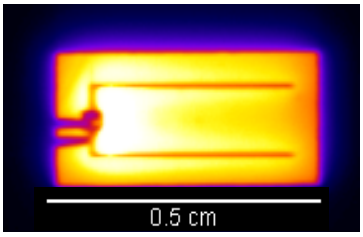

16mA 693mV 2s

	Min	Max	Average
1st meas.	2202	39241	26499
2nd meas.	2146	38247	25809
3rd meas.	2181	38547	26006
4th meas.	2230	38665	26103
5th meas.	2226	38701	26159
Average	**2197**	**38680**	**26115**
		%deviation= 2.6 %	

Figure 3.10: Different EL images and current injection

The percentage deviation can be seen on Table 1. Since the Si-CCD camera is quite prone to read out noise, therefore, more counts means less noise and better accuracy. Moreover, Si-CCD cameras have linear response, meaning that the number of counts collected in the pixels is proportional to the exposure time of the measurement [46]. Thus, greater counts can be achieved by doing long integration time. At Solliance, the method is advisable to have counts around 40000-60000 for a better quality image. Although in this experiment, there is a rare coincidence that the counts of around 12000

have a lower percentage error. This was indeed an unusual situation that has been found during this work.

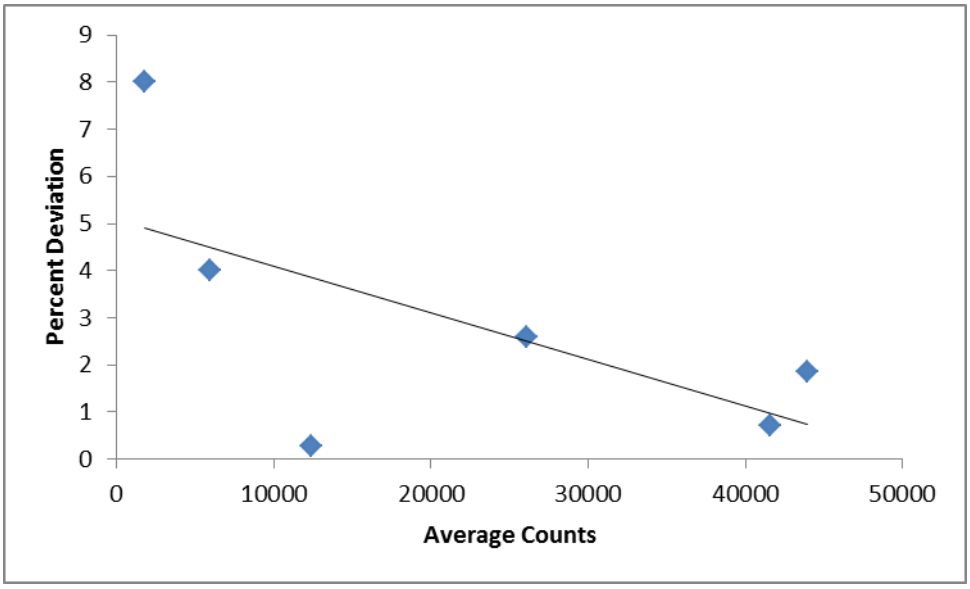

Figure 3.11: Percentage deviation trend measured at ECN

3.1.2 Time Integration and SNR

The detector or the camera accumulates the photons (as known as counts) that are emitted from the sample over time in luminescence procedure; thus, photon flux highly depends on the integration time. This integration time also affects signal-to-noise ratio (SNR), which can be improved by increasing the time. The higher the SNR is, the accurate the image, since it would be less distorted. For each luminescence application, the integration time should be optimized by the user. Although it is said that the longer integration time can improve the SNR, however in practice, the maximum exposure time is limited by the capacity of the used detector or camera. The camera has a limit of around 65000 counts, and if it exceeds this limit, the pixel will become saturated. This is called *Saturation Charge Level* [47]. Moreover, it is also important to know that the temperature of the camera needs to be in control if the integration time is set to be long. This is important because the photon detection by the camera is highly dependent on the temperature. As the instrument warms up during operation, this affects the consistency of the luminescence signal over time. Maintaining a set temperature of 20°C will keep the instrument stable, avoiding drifting luminescence signals. The Greateyes system uses a thermoelectric cooler that operates according to *Peltier* effect. The effect creates a temperature difference by transferring heat between two electrical junctions. A voltage is applied across joined conductors to create an electric current. When the current flows through the junctions of the two conductors, heat is removed at one junction and cooling occurs. Heat is deposited at the other junction.The main application of the Peltier effect is cooling. However the Peltier effect can also be used for heating or control of temperature. In every case, a DC voltage is required [48].

For a silicon CCD camera, dark noise is the most undesirable signal components that makes it a huge drawback. Dark noise occurs from statistical variation in the number of electrons thermally generated within the silicon structure of the CCD, which is independent of photon-induced signal, but highly dependent on device temperature. The generation rate of thermal electrons at a given CCD temperature is referred to as *dark current*. Consequently, cooling the CCD reduces the dark current dramatically, and in practice, high-performance cameras are usually cooled to a temperature at which dark current is negligible over a typical exposure interval [49]. Therefore, for the sake of the noise ratio, the silicon CCD camera is cooled to 20°C.

4.0 Methodology

EL imaging is an emerging conventional tool for quality assurance in solar cell characterization. As previously stated, EL is non-destructive and easy to apply, since the procedure only needs camera, contacting probes, and power supply. One of the most important properties of a solar cell that is observable with luminescence imaging is the local series resistance R_s that can influence the performance of solar cell, affecting its fill factor and efficiency. According to Haunschild, the origin of high R_s values from I-V characterization are in most cases not homogeneously distributed, but may vary laterally [50]. There has been several researches to obtain R_s values from PL EL images, such as, Trupke (2007), Ramspeck (2007), Hinken (2008), etc. All luminescence-based series resistance methods do the transfer from the luminescence image to voltage mapping, and eventually series resistance mapping. These researches have been based on silicon solar cell and this thesis aims to transfer these methods to thin film PV, especially CIGS. EL analysis in thin film cells has a great potential to reveal the film properties. In addition, this thesis will only focus on transferring EL image to voltage distribution mapping.

4.1 Voltage dependence on EL images

The intensity of the emitted photons is related to the radiative band-to-band recombination method, material and optical properties of the cell material but there is a strong dependence on the applied voltage. In addition, the EL intensity is proportional to the excess carrier density within the sample [50]. The approach used in this thesis to compute voltage mapping is Haunschild's method, since it requires only two EL images taken at different voltages. As mentioned before, the method requires conversion from electroluminescence signal to local voltage mapping. Current is injected to a cell in order to stimulate radiative recombination, while the silicon CCD camera captures the EL emission of the solar cell. The junction voltage varies across the surface of the sample, but it is not wavelength dependent, therefore, the local junction voltage can be measured through spatially resolved electroluminescence.

The spatially resolved EL analysis makes use of the relation between the local EL emission $\Phi_{el}(E)$ and the local junction voltage. The combination of Eq. 5 and Eq. 9 gives the measured local luminescence in the EL case. In these equations, exponential function local voltage V_i can be taken out of the integrals, and when combined, the local luminescence is expressed as below.

$$\emptyset i = Ci * \exp\left(\frac{Vi}{Vt}\right) \tag{11}$$

Assuming injection independent charge carrier recombination properties, the local luminescence signal $\emptyset i$ at pixel $i = (x, y)$ scales exponentially with the local internal voltage Vi and it is also proportional to $\exp(\frac{Vi}{Vt})$, with Vt as the thermal voltage, Ci is the calibration constant which is related to optical and material properties of the camera and solar cell. This equation holds for conditions where Vi is larger than Vt [26]. Ci relates the local luminescence intensity to the local junction voltage

and is determined under low current injection or applied voltage conditions for EL. In this case, voltage gradients are negligibly small and the local internal voltage Vi can be assumed equal to the applied voltage V_{appl} for every position of the cell. This procedure usually requires long integration time for the current to be distributed throughout the sample and it is assumed to be homogeneous [51]. Once Ci is calculated from the low power image, this calibration constant is then used to calibrate images at any excitation level to find its local junction voltage by

$$Vi = Vt * LN(\frac{\emptyset i}{Ci}) \quad (12)$$

However, this method has been practiced on the silicon solar cells and in this thesis, the aim is to transfer this methodology to thin film solar cells. In this thesis, the calculation is done in Microsoft Excel and the image software used is ImageJ. ImageJ transforms the image to a data file that shows the intensity per pixel, which is then copied to the Excel file where the calculation can be performed.

4.2 Measurements of Low and High Power

With the Greateyes system, EL procedure is performed on a CIGS cell with an area of 0.5cm^2. According to the procedure, a low power image is needed to obtain a calibration constant. To choose the low current to be injected to the cell, in this thesis is assumed to be 10% of the short circuit current of the cell. This CIGS sample has I_{SC} of 16mA; therefore, a current of 1.6mA is injected to the cell (with a reading of voltage of 581mV) for 70 seconds. As mentioned before, long integration time is necessary for low current to distribute a constant voltage across the cell. From Fig. 4.1 of low power image, gray value defines as the counts. It is visibly noticeable that the luminescence signal throughout the cell is constant and it is proven by the signal profile that is measured along the line (blue). When the current injected is small, the voltage drop can be considered negligible, thus, creating an even distribution of voltage across the cell. This step is important since the calibration constant Ci can be calculated from equation (11). In addition, this lower power image possesses a homogeneous signal, therefore, Vi can be assumed to be the voltage applied to the solar cell, which is 581mV.

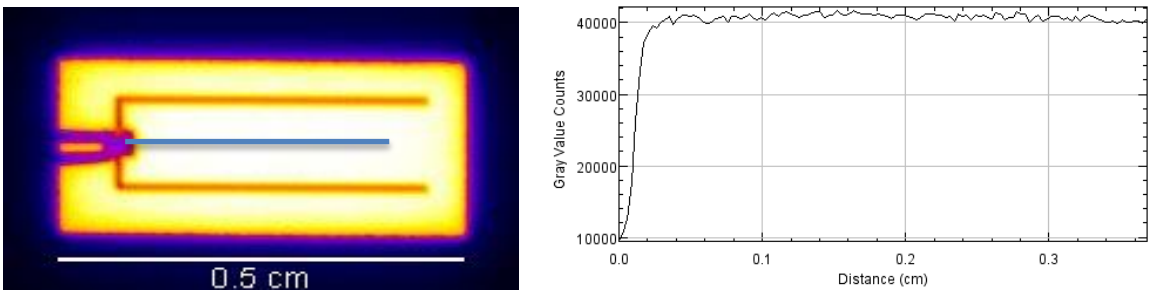

Figure 4.1: EL image of 1.6mA injection (left) and intensity profile (right)

The second measurement needed is the high power image. Fig. 4.2 is an EL measurement taken with 16mA injected and a voltage reading of 681.4mV for 5seconds. The high power image is needed to see the voltage-mapping image. As seen from the intensity profile, the signal decreases just after the

busbar, which means, the high power image possesses high voltage drop, caused by the series resistance, yielding a non-homogeneous signal image. The goal is to be able to map the voltage distribution of the high power image.

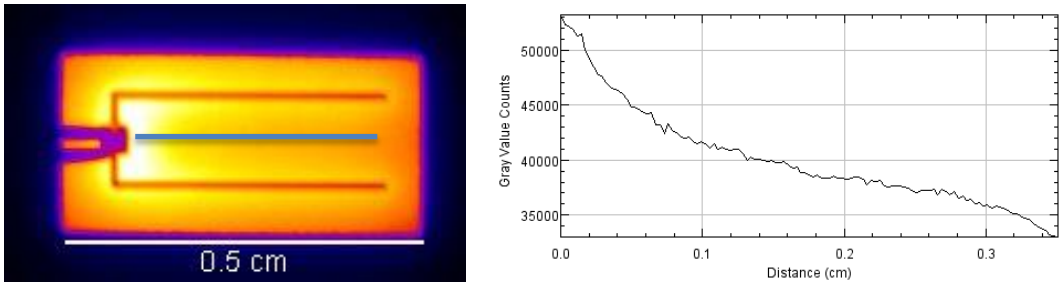

Figure 4.2: EL image of 16mA injection

Once the image is obtained, utilizing ImageJ, the image is converted to data file. This data file is then copied to Microsoft Excel for calculation purposes. In Microsoft Excel, the signal data is calculated per pixel.

4.3 Voltage Distribution Calculation

As mentioned before, the low power image is used to calculate the Ci, with the condition $Vi = Vapplied$. This Ci is transferred to equation (12) for voltage distribution image. Fig. 4.3 shows the result from the calculation done on 1.6mA and 16mA images. However, the cell is barely visible since the upper part of the image has higher intensity than the cell.

The assumption of equation (11) was that the Vi is constant throughout the cell. However, during the calculation to find Ci using this equation, the whole image (including the non-active area) was taken into account and it was assumed to have a voltage applied of 581mV, when in fact the non-active area had no voltage applied. Due to the error in the voltage distribution calculation, the non-active area shows a higher voltage than the cell. Essentially, the non-active area is not the area of interest, but due to this error, there is no visibility of the measured cell. Therefore, the signal of non-active area from the low power measurement should be altered in order to have approximately the same signal as the cell area.

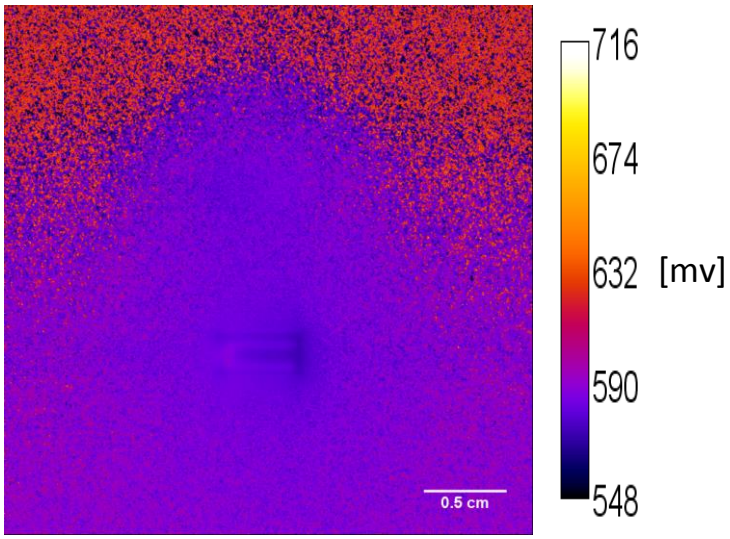

Figure 4.3: Local voltage mapping

4.4 Modification Image

The assumption of an equal voltage distribution throughout the whole cell was made for the low power measurement. Therefore, a modification image is only needed for the low power image. The modified image will change the non-illuminated area signal to be more or less the same as the cell's signal.

The procedure is to take the average value of signal from the center of the cell and set it as a reference, because it is assumed that the voltage on the center of the cell is constant. Then, if the signal of pixel position i is less than half of the reference, it will be replaced by the reference value. If not, the signal is unchanged. Below is the command that is written in the Excel.

$$= If\left(LowPowerImage!A1 < \frac{Ref}{2}, Ref, LowPowerImage!A1\right)$$

With this modification image, the non-active area would have the same signal as the average of the cell's intensity. The low power modification image is then used to calculate the calibration constant.

Then, equation (12) is used to get the values of local voltage in every pixel i. Fig. 4.4 is the voltage distribution of 16mA using the modification image. With the modification of the low power image, the active cell area can be distinguished. The intensity is then adjusted to display just the values from the minimum to the maximum intensity that the cell holds.

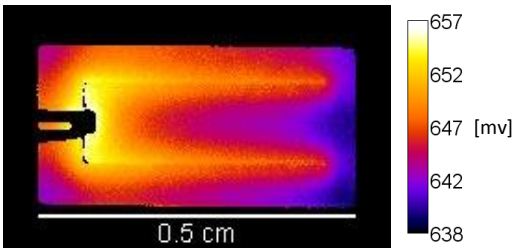

Figure 4.4: Voltage distribution of 16mA

The voltage distribution of 16mA injected has a voltage range of 638-657mV applied across the cell. However, when the measurement was done through injecting 16mA to the cell (for the high power measurement), the voltage reading on Keithley power supply showed 681.4mV. There is a 24mV difference between the voltage reading of Keithley and the calculated voltage. To evaluate and analyze the inaccuracy, a voltage difference test is done.

4.5 Voltage Difference Test

In order to analyze where the missing voltage goes, EL is performed on a single cell with current of 1.6mA, 3mA, 4mA, 6mA, 8mA, 10mA, 12mA, 14mA and 16mA. Using equation (11), 1.6mA is used as a calibration image, while equation (12) is used to perform voltage distribution calculation on the other images. Fig. 4.5 shows the voltage distribution and voltage scale of each different current. From the figures, the maximum voltage from each image is obtained.

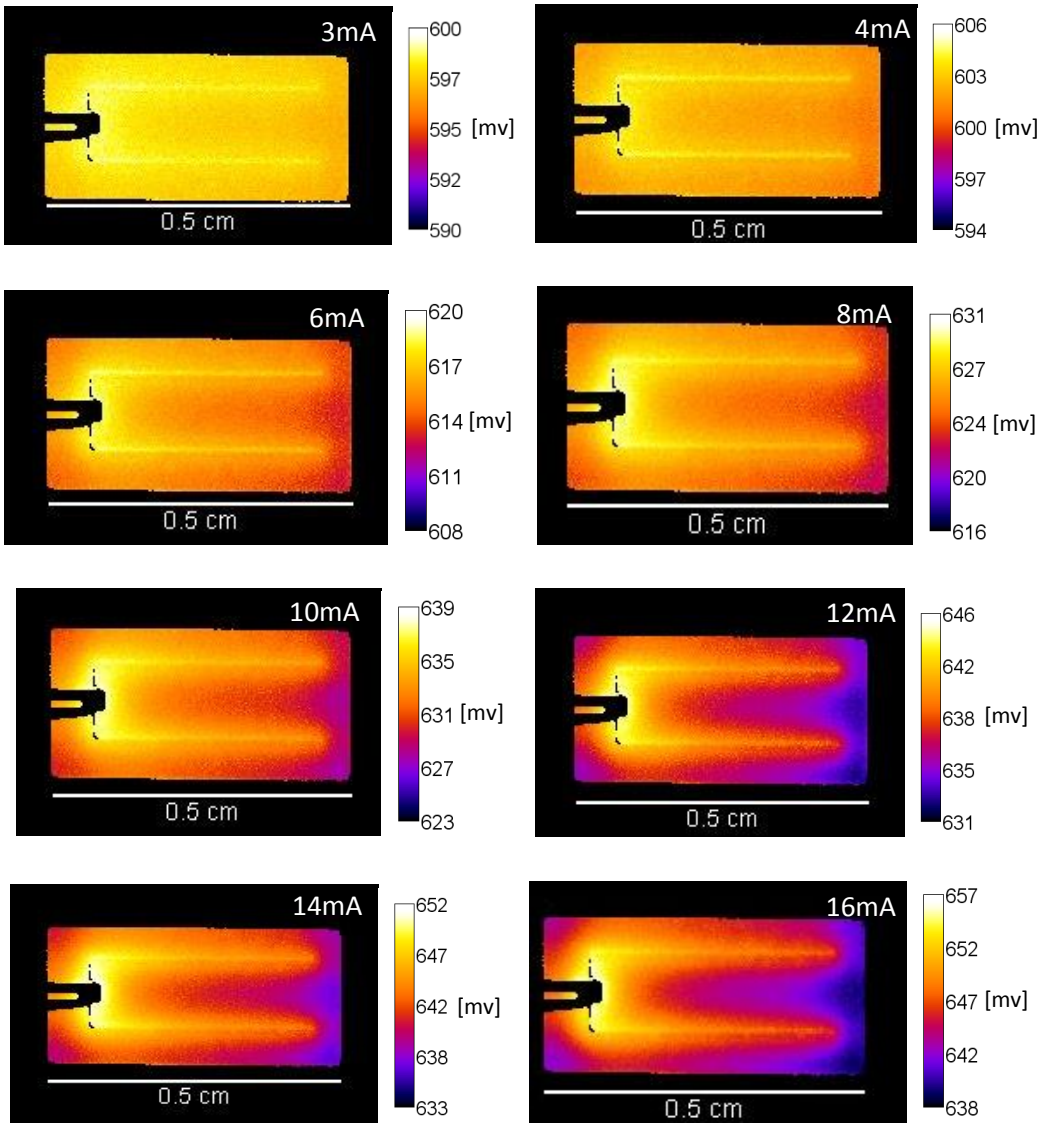

Figure 4.5: Voltage distribution for different current injection

Table 2: Data for voltage difference

Current [mA]	Keithley [mV]	Image [mV]	Difference [mV]
3	602	600	2
4	613.8	606	7.8
6	631.2	620	11.2
8	644.5	631	13.5
10	655.5	639	16.5
12	665.1	646	19.1
14	673.7	652	21.7
16	681.4	657	24.4

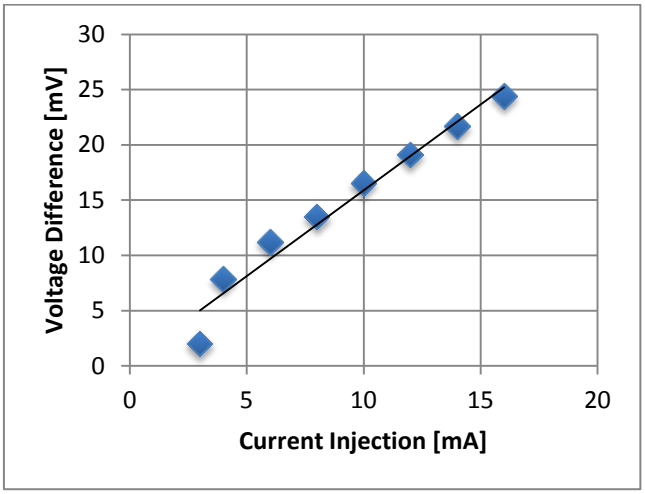

Figure 4.6: Voltage difference vs. Current Injection graph

As seen in Fig. 4.6, it is clear that for higher current injection, the greater the voltage difference between the calculated and the measured values. With Ohm's Law, resistance can be calculated from each point, since there is a voltage difference between the calculated (reading from image) and the measured (reading from Keithley) at every current injection. For each current, the calculated resistance is around 1.5Ω to 1.8Ω. The difference between the calculated and the measured voltages is due to the series resistance within the cell or even from the contact resistance of the probes. However, it is highly possible that the back contact's (molybdenum) series resistance dominates it, which is not detectable by EL procedure, because the intensity gradient of the image through the use of EL shows the series resistance of the top surface (TCO layer).

The non-uniformity of the luminescence signal is tightly related with the series resistance of the TCO. In the case of thin film solar cells, series resistance in TCO plays a crucial role in effective collection of photo-generated carriers (in other words, effective injection of minority carriers in EL measurement) to get high performance [52]. Therefore, it is not possible to determine the series resistance in the back contact, or the molybdenum for this case. However, the local determination of the series resistance is of greatest interest to solar cell analysis because the back and front contact, as well as the finger resistances make up the largest part of the total series resistance.

4.6 Scaling Up to Bigger Cells

The experiment has been done on a 0.5cm^2 CIGS cell for the purpose of trials. In the end, the research was to conduct this method into different sizes of solar cells. Therefore, transferring the method into a larger area is essential. The new area that was experimented on is of 3cm^2 and 5cm^2. Initially, both cells were measured through EL technique.

4.6.1 Voltage Mapping of 3cm^2

For this 3cm^2 area, the current will be injected to produce a low power and a high power image. The low power image was injected with a small current with a longer integration time. With 8.3mA current injected in 200s, the voltage measured was 500mV. Meanwhile, the high power image is injected with current of 75mA in 3s, and the voltage was measured 800mV. The low power and high power image can be seen in Fig. 4.7. The low signal (bottom left corner) on both Fig. 4.7 (a) and (b) illustrates the series resistance of the cell. However, the low power image can still be used since the signal gradient from high signal to low signal isn't that significant (seen in Fig. 4.8). Therefore, it can still be assumed that the voltage throughout the cell is constant. Using modified image, equation (11) and (12), the voltage mapping image is obtained.

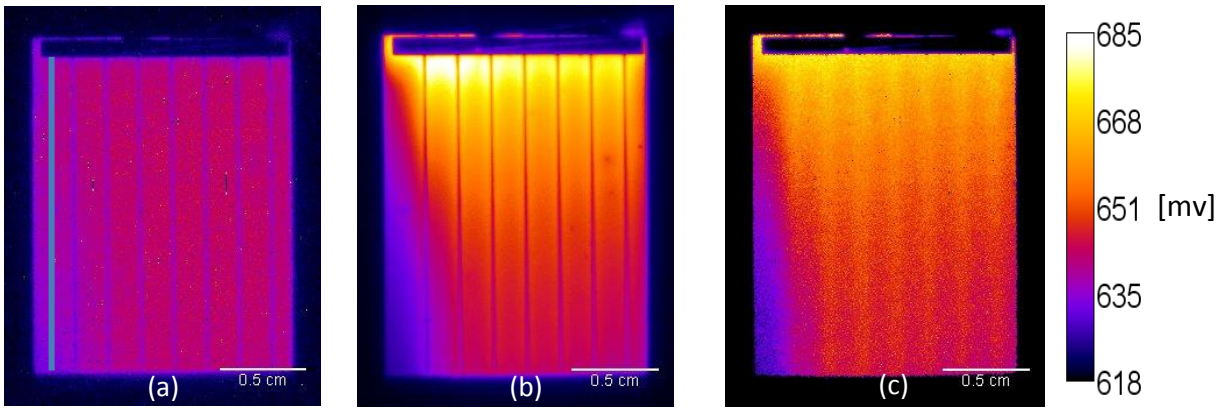

Figure 4.7: Low power image (a), High power image (b), and Voltage mapping and its scale (c)

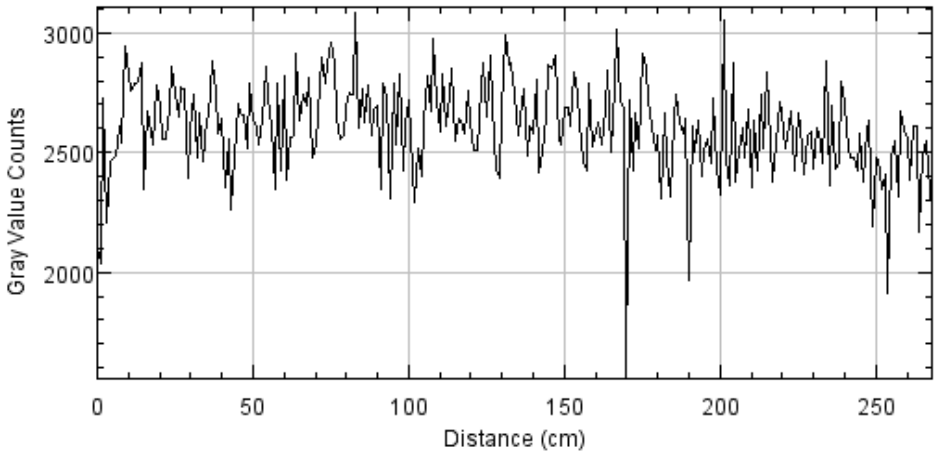

Figure 4.8: The signal distribution of low power image (Fig. 4.7 (a))

Fig. 4.7 illustrates that the method is successfully done on a 3cm^2 CIGS cell. Fig. 4.7 (c) illustrates the voltage mapping that has a maximum voltage of 685mV. Again, there is a difference between the measured and the calculated voltage, just like explained in Ch. 4.5. In this experiment, the voltage difference is 800mV-685mV = 115mV. Using the Ohm's law, it is calculated that the cell has a resistance of 1.53Ω. Since this is done on a different substrate, resistance is different than the one measured in Ch. 4.5.

4.6.2 Voltage Mapping of 5cm^2

Scaling up the area of the cell for EL procedure was predicted to be problematic for larger areas. Due to the low current that will not reach the end of the cell when applied on the busbar. Setting a long integration time for the procedure on a long cell would also give inaccuracy, since temperature of the system and the cell is related to the efficiency of the detector. The assumption for calibration factor is to have approximately constant voltage throughout the cell, however, with a longer cell, this assumption may not hold. There would always be some resistances within the cell while injecting current through a long cell. Fig. 4.9 confirms that with EL itself, the low current injection is not possible to do with this 5cm^2 CIGS cell; cell was injected 10mA 500mV in 500s. The EL image shows noisy and non-homogeneous signal. Hence, it was theorized that a combination of PL and EL was needed to proceed with this experiment. The combination of PL and EL was hypothesized to give a homogeneous light emission source across the sample, while the Keithley measures current and voltage.

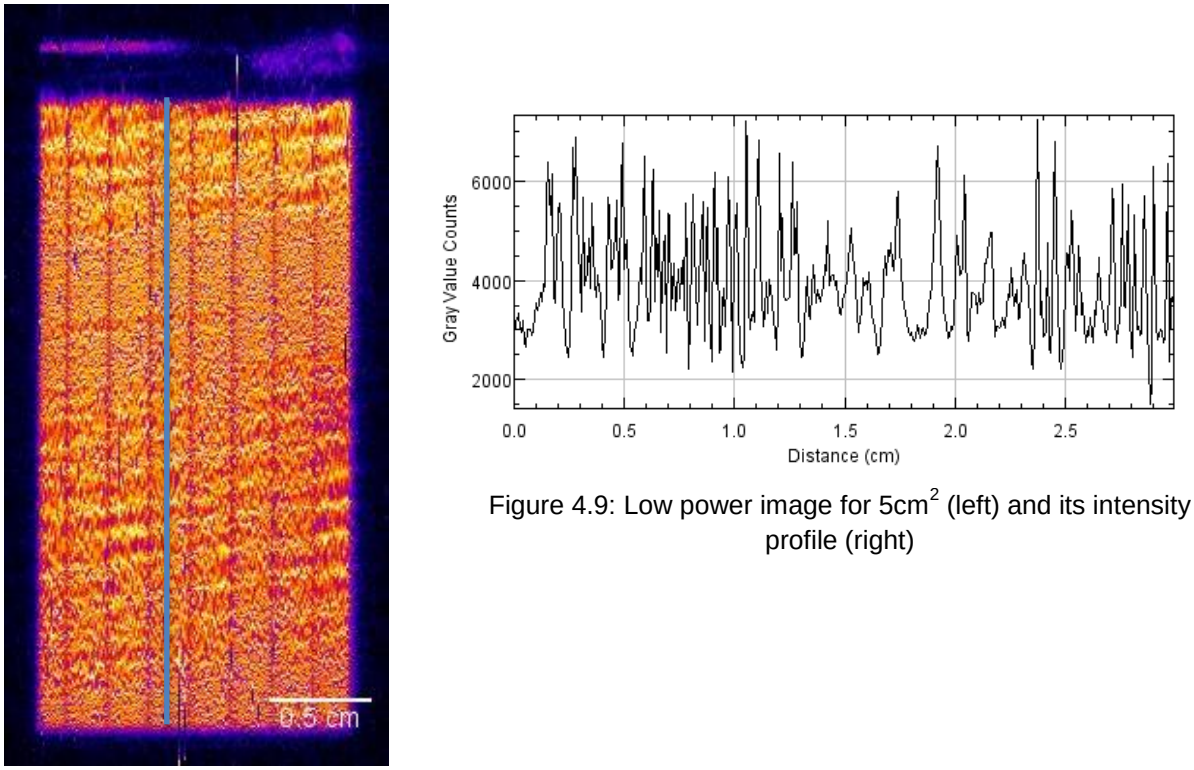

Figure 4.9: Low power image for 5cm^2 (left) and its intensity profile (right)

4.6.3 Combination of EL PL

Fig. 4.10 (left) shows the PL image taken with LED power of 2A for 30 seconds. The LED power is set to a low intensity in order to provide low power image for calibration factor calculation. The calibration factor calculation requires a uniform signal, which represents a uniform voltage distribution since the intensity of the emitted photons depends on the applied voltage (in equation (11), V_i is assumed to be equal as voltage applied to the cell). Fig. 4.10 displays the intensity profile of the image and it is evident that the cell possess a non-uniform distribution of signal. Meaning, this image cannot be used to calculate the calibration constant, since V_i is not equal to the voltage applied. V_{appl} was measured by Keithley to be in the range of 630-638mV, which proves that V_i cannot be constant. In conclusion, this procedure is also challenging since the image that is required to calculate a calibration constant needs to have a constant voltage, allowing a negligible amount of series resistance. In addition, the uniformity of light causes an additional problem, since the LEDs are adjustable, it is possible that the emission of the light is not as homogeneous. The signal differs from 40000 counts to around 24000 counts. Therefore, PL/EL method is not a reliable method to use when scaling up the solar cell.

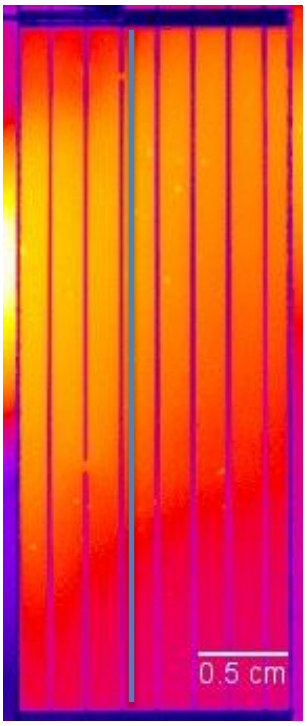

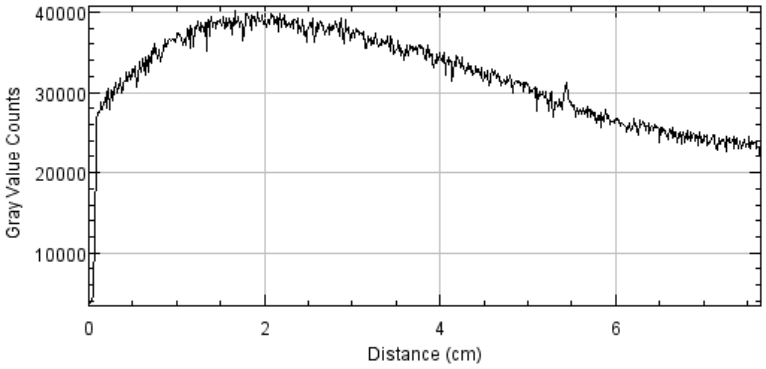

Figure 4.10: Low power image using a combination of PL and EL (left) and its intensity (right)

5.0 Conclusions, Discussion and Future Work

Luminescence imaging is highly suitable for quality control of processing procedures, especially the control of homogeneous layer deposition and the proper lateral function of solar cells by identification of local defects, for example, by varying the applied bias voltage, further information can be resolved with regard to the resistive losses within the cell. The EL imaging techniques and the image processing requires further improvement in order to obtain quantitative results like cell's voltage distribution and series resistances. This includes improving the signal to noise (S/N) ratio of images at low voltage levels to improve accuracy. Further enhancements in the image-processing program are also necessary to speed up the processing of the high resolution images. Microsoft Excel and ImageJ were used as image processing tool, which most often slowed down the computer's processor due to large data that has to be analyzed.

In this thesis, different measurements are done on the Greateyes luminescence system in order to understand the device further. We looked into how reliable and reproducible it is and have concluded that in order to have an accurate image, long integration time and high counts are necessary, which is around 40000-60000 counts. Next, we have analyzed and demonstrate that voltage-mapping procedure of silicon solar cell can be transferred to thin film cells. This procedure is done using equation (11) to produce a calibration constant from a low power image with the assumption of a homogeneous voltage distribution; and equation (12) is used to calculate the voltage distribution of the high power image. But, there is a voltage difference between the measured (reading of Keithley) and calculated (scale bar of voltage image) maximum voltage. We are assuming that the series resistance within the CIGS causes the voltage difference between the calculated image and the voltage that is measured by Keithley. However, there is a strong possibility that the main resistance comes from the back contact. Furthermore, while this EL method is confirmed for small thin films ($0.5cm^2$ – $3cm^2$), transferring this method to long thin film cell above $5cm^2$ area was not successful. Series resistances are still dominating while doing low injection of EL procedure, in a short or long integration time. Thus, a combination of EL and PL was needed, in the aim to get a homogenous signal throughout the cell. Unfortunately, this procedure also gives a non-homogeneous signal throughout the cell. Therefore, silicon's voltage-mapping procedure can be transferred to small thin films but cannot be scaled up to a large area.

Future work regarding this thesis is to develop a new method of calibration constant that is based on non-homogeneous signal thin films. The voltage-mapping depends on the calibration constant that is required a homogeneous signal. Therefore, it is important to tackle the calibration constant for non-uniform signal. Afterwards, transforming the voltage-mapping to a series resistance image would be essential, since the series resistance has a great effect on the luminescence intensity. This would give us more degree of freedom in the analysis of the homogeneity of the thin films.

Bibliography

[1] International Energy Agency, "Energy and Climate: State of Play," in *Energy and Climate Change*, France, 2015, p. 22.

[2] J. Funk and C. Magee, Exponential Change: What drives it? What does it tell us about the future?, 2015.

[3] Greateyes, [Online]. Available: http://www.greateyes.de/greateyes_LumiSolarCellOverview_en.html. [accessed on 25.10.2016]

[4] W. C. Wee, "Molybdenite - the New Semiconductor Material?," 2 02 2012. [Online]. Available: http://www.hardwarezone.com.sg/tech-news-molybdenite-new-semiconductor-material. [Accessed 25.10.2016].

[5] A. Bayoumi and N. Rafat, "Band Theory: E-K Diagram, Energy Gaps and Effective Mass," Cairo, 2015.

[6] B. V. Zeghbroeck, "Principles of Semiconductor Devices," 12 2004. [Online]. Available: http://ecee.colorado.edu/~bart/book/book/chapter4/ch4_6.htm. [accessed on 25.10.2016]

[7] Haug and Franz-Josef, "Semiconductors," [Online]. Available: http://www.superstrate.net/pv/optical/.[accessed on 25.10.2016]

[8] T.-M.-H. Tran, "Quantitative analysis of spatially resolved electroluminescence of CIGS and a-Si:H thin-film solar cells and modules".

[9] D. Hinken, K. Ramspeck, K. Bothe and B. Fischer, "Series resistance imaging of solar cells by voltage dependent electroluminescence," *Applied Physics Letters,* vol. 91, p. 182104.

[10] M. Theelen, Degradation of Solar Cells, Delft, 2015.

[11] TDK-Lambda Americas Inc, "Genesys™ 1U 750W and 1500W Programmable DC Power Supply," TDK Lambda, [Online]. Available: http://www.us.tdk-lambda.com/hp/product_html/genesys1u.htm. [accessed on 25.10.2016]

[12] KEPCO, INC, "Bipolar 4-quadrant, Analog/Digital/Local Control, Ultra Low Ripple/Noise," Kepco, [Online]. Available: http://www.kepcopower.com/bop.htm. [accessed on 25.10.2016]

[13] Direct Industry , "Keithley AC/DC power supply / rectifier / benchtop / low-voltage," [Online]. Available: http://www.directindustry.com/prod/keithley-instruments/product-1438-1039153.html. [accessed on 25.10.2016]

[14] SunShot, "PV Performance," [Online]. Available: https://pvpmc.sandia.gov/modeling-steps/2-dc-module-iv/diode-equivalent-circuit-models/. [Accessed 29.10.2016].

[15] PV education, "Quantum Efficiency," [Online]. Available: http://www.pveducation.org/pvcdrom/quantum-efficiency. [accessed on 25.10.2016]

[16] A. Shah, "Global Issues: Climate Change and Global Warming," 2015. [Online]. Available: http://www.globalissues.org/issue/178/climate-change-and-global-warming. [Accessed 22 10 2016]. [accessed on 25.10.2016]

[17] REN21, "RENEWABLES 2016: GLOBAL STATUS REPORT," 2016.

[18] U.S. Energy Information Administration, "International Energy Outlook 2016," U.S. Department of Energy.

[19] National Renewable Energy Laboratory, "Types of Renewable Energy," [Online]. Available: http://www.renewableenergyworld.com/index/tech.html. [Accessed 16 09 2016]. [accessed on 25.10.2016]

[20] D. Abou-Ras, T. Kirchartz and U. Rau, Advanced Characterization Techniques for Thin Film Solar Cells, Weinheim: Wiley-VCH, 2010.

[21] IPCC, "Special Report on Renewable Energy Sources and Climate Change Mitigation".

[22] S. Heckeroth, "Mother Earth News: The Original Guide to Living Wisely," 3 2010. [Online]. Available: http://www.motherearthnews.com/renewable-energy/solar-power/thin-film-solar-zmaz10fmzraw. [accessed on 25.10.2016]

[23] A. A. M. Sayigh, "Renewable Energy," *Special Issue World Renewable Energy Congress Renewable Energy, Energy Efficiency and the Environment,* vol. 8, no. 1-4.

[24] Hinken, K. Bothe and David, "Quantitative Luminescence Characterizaiton of Crystalline Silicon Solar Cells," in *Advances in Photovoltaics Part 2*, vol. 89, G. P. W. a. E. R. Weber, Ed., pp. 259-339.

[25] T. Fuyuki, H. Kondo, T. Yamazaki, Y. Takahashi and Y. Uraoka, "Photographic surveying of minority carrier diffusion length in polycrystalline silicon solar cells by electroluminescence," *Applied Physics Letters,* vol. 86, p. 262108, 2005.

[26] T. Potthoffy, K. Bothe, U. Eitner, D. Hinken and M. Kontges, "Detection of the voltage distribution in photovoltaicmodules by electroluminescence imaging," *PROGRESS IN PHOTOVOLTAICS: RESEARCH AND APPLICATIONS,* vol. 18, pp. 100-106, January 2010.

[27] HyperPhysics, [Online]. Available: http://hyperphysics.phy-astr.gsu.edu/hbase/Solids/Fermi.html. [accessed on 25.10.2016]

[28] "Electronic Tutorials," AspenCore, Inc, [Online]. Available: www.electronics-tutorials.ws/diode/diode_2.html.

[29] Y. Augarten, "Extension of Photoluminescence Imaging Characterisation," South Wales, 2012.

[30] Jojo, "Understanding the PN Junction," 21 07 2014. [Online]. Available: http://www.circuitstoday.com/understanding-the-pn-junction. [Accessed 25.10.2016].

[31] D. K. Skorupska, "Optical Properties of Semiconductors," [Online]. Available: http://www.uwyo.edu/cpac/_files/docs/kasia_lectures/3-opticalproperties.pdf. [accessed on 25.10.2016]

[32] M. Zeman, "Reading 3: Semiconductor materials for solar cells," [Online]. Available: https://ocw.tudelft.nl/course-readings/solar-cells-r3-semicon-materials/. [Accessed 26 10 2016].

[33] "PV Education," [Online]. Available: http://www.pveducation.org/pvcdrom/pn-junction/types-of-recombination#footnote2_o84lh9x. [Accessed 27 July 2016].

[34] T. Trupke, R. Bardos, M. Abbott, P. Würfel, E. Pink, Y. Augarten, F. Chen, K. Fisher, J. Cotter, M. Kasemann, M. Rüdiger, S. Kontermann, M. Schubert, S. Glunz, W. Warta, D. Macdonald, J. Tan, A. Cuevas, J. Bauer, R. Gupta, O. Breitenstein, T. Buonassisi, G. Tarnowski, A. Lorenz, H. Hartmann, D. Neuhaus and J. Fernandez, "Progress with Luminescence imaging for the Characterization of Silicon Wafers and Solar Cells," *22nd European Photovoltaic Solar Energy Conference,* pp. 3-7, September 2007.

[35] T. Trupke and P. Würfel, "Luminescence Imaging of Solar Cells".

[36] K. N. Zaunbrecher, S. W. Johnston and J. R. Sites, "Identification and Analysis of Distinct Features in Imaging Thin-film Solar Cells," in *IEEE Photovoltaic Specialists Conference*, Austin, 2012.

[37] T. Lavrenko, F. R. Runai, Y. Wang, M. Teukam and T. Walter, "Advanced Luminescence Imaging of CIGS Solar Cells," in *27th European Photovoltaic Solar Energy Conference and Exhibition*, 2012.

[38] A. Helbig, T. Kirchartz, R. Schaeffler, J. H. Werner and U. Rau, "Electroluminescence Analysis of CIGS Thin Film Modules".

[39] U. Rau, "Superposition and Reciprocity in the Electroluminescence and Photoluminescence of Solar Cells," *IEEE Journal of Photovoltaics,* vol. 2, p. 169, 2012.

[40] A. Polman, M. Knight, E. C. Garnett, B. Ehrler and W. C. Sinke, "Photovoltaic materials: Present efficiencies and future challenges," in *Science*.

[41] Hedayati and M. Keshavarz, "Techomat," 8 July 2015. [Online]. Available: https://techomat.com/2015/07/08/a-simple-introduction-to-thin-film-solar-cells/.[accessed on 25.10.2016]

[42] P. Salome, V. Fjallstrom, A. Hultqvist and M. Edoff, "Na Doping of CIGS Solar Cells Using Low," *IEEE Journal of Photovoltaic,* vol. 3, no. 1, 2013.

[43] M. Schmidt and U. Rau, "Electronic properties of ZnO/CdS/Cu(In,Ga)Se2 solar cells - aspects of heterojunction formation," *Thin Solid Films,* vol. 387, pp. 141-146.

[44] Y. Galagan, B. Zimmermann, E. W. Coenen and M. Jørgensen, "Current Collecting Grids for ITO-Free Solar Cells".

[45] M. Rouse, "TechTarget," [Online]. Available: http://searchstorage.techtarget.com/definition/charge-coupled-device. [accessed on 25.10.2016]

[46] K. R. Spring, T. J. Fellers and M. W. Davidson, "Introduction to Charge-Coupled Devices (CCDs)," [Online]. Available: https://www.microscopyu.com/digital-imaging/introduction-to-charge-coupled-devices-ccds. [Accessed 24 10 2016]. [accessed on 25.10.2016]

[47] T. J. Fellers and M. W. Davidson, "CCD Saturation and Blooming," 12 02 2016. [Online]. Available: https://micro.magnet.fsu.edu/primer/digitalimaging/concepts/ccdsatandblooming.html. [Accessed 24.10.2016].

[48] II-VI Marlow, "How Do Thermoelectric Coolers Work," [Online]. Available: http://www.marlow.com/resources/general-faq/6-how-do-thermoelectric-coolers-tecs-work.html. [accessed on 25.10.2016]

[49] Davidson, T. J. Fellers and M. W., "CCD Noise Sources and Signal-to-Noise Ratio," National High Magnetic Field Laboratory, [Online]. Available: http://hamamatsu.magnet.fsu.edu/articles/ccdsnr.html. [accessed on 25.10.2016]

[50] J. Haunschild, M. Glatthaar, M. Kasemann, S. Rein and E. R. Weber, "Fast Series resistance imaging for silicon solar cells using electroluminescence," Phys. Status Solidi RRL 3, 2009.

[51] M. Glatthaar, J. Haunschild, M. Kasemann, J. Giesecke, W. Warta and S. Rein, "Spatially resolved determination of dark saturation current and series resistance of silicon solar cells," Physics Status Solidi RRL 4, 2010.

[52] Fuyuki, A. Tani and Takashi, "Direct Assessment of Series Resistance in Thin Film Solar Cells Utilizing Electroluminescence," IEEE.

[53] J. M. Raguse, "ELECTROLUMINESCENCE OF THIN-FILM CDTE SOLAR CELLS AND MODULES," Colorado, 2015.

[54] A. Srivastava, "Observation of Dark Excitons," in *Micro-Photoluminescence Spectroscopy of Excitons in Individual Single Walled Nanotubes*, pp. 42-45.

[55] D. Heiman, "Photoluminescence Spectroscopy," 2004.

[56] U. Rau, "Reciprocity relation between photovoltaic quantum efficiency and electroluminescent emission," PHYSICAL REVIEW B, 2007.

[57] D. Amaury, L. Laurent and G. Jean-François, "Characterization of solar cells," *Photonics Energy,* vol. 027004, pp. 1-8, 2012.

[58] C. Donolato, "A reciprocity theorem for charge collection," Bologna, 1984.

[59] B. Streetman and S. Banerjee, "Excess Carriers in Semiconductors," in *Solid State Electronic Devices*, Prentice Hall, 2005.

[60] U. Rau and T. Kirchartz, "Electroluminescence analysis of high efficiency Cu (In , Ga) Se 2 solar cells," 2007.

[61] H. F. Dam, Larsen-Olsen and T. Trofod, "How to Measure Solar Cell," plasticphotovoltaics.org, [Online]. Available: http://solideas.comwww.solideas.com/papers/GPS25_1992_51.pdf. [accessed on 25.10.2016]

[62] J. Carstensen, G. Popkirov, J. Bahr and H. Foll, "CELLO: an advanced LBIC measurement technique for solar cell local characterization," *Solar Energy Materials & Solar Cells,* vol. 76, pp. 599-611.

[63] K. Ramanathan, F. Hasoon, H. Al-Thani, J. Alleman, J. Keane, J. Dolan, M. Contreras, R. Bhattacharya and R. Noufi, "Recent Progress in CIGS Thin Film Solar Cell Research at NREL," in *NCPV Program Review Meeting*, 2001.

[64] O. Breitenstein, J. Rakotoniaina, M. Kaes, S. Seren, T. Pernau, G. Hahn, W. Warta and J. Isenberg, "LOCK-IN THERMOGRAPHY - A UNIVERSAL TOOL FOR LOCAL ANALYSIS OF SOLAR CELLS," in *20th European Photovoltaic Solar Energy Conference*, Barcelona, 2005.

[65] D. Baugh, "Introduction to Band Theory". http://www.imagesco.com/articles/photovoltaic/photovoltaic-pg4.html. [accessed on 25.10.2016]

[66] S. Fischer, J. C. Goldschmidt, P. Löper, G. H. Bauer, R. Brüggemann, K. Krämer, D. Biner, M. Hermle and S. W. Glunz, "Enhancement of silicon solar cell efficiency by upconversion: Optical and electrical characterization," *Applied Physics,* vol. 108, p. 044912, 16 07 2010.

Appendices

A1 Circuit Model

To characterize a solar cell, some theory of how the equivalent circuit diagram for a solar cell needs to be understood. Equivalent circuit models define the entire I-V curve of a cell, module, or array as a continuous function for a given set of operating conditions. One basic equivalent circuit model in common use is the single diode model with 5 parameters model, illustrated in Fig. A.1.

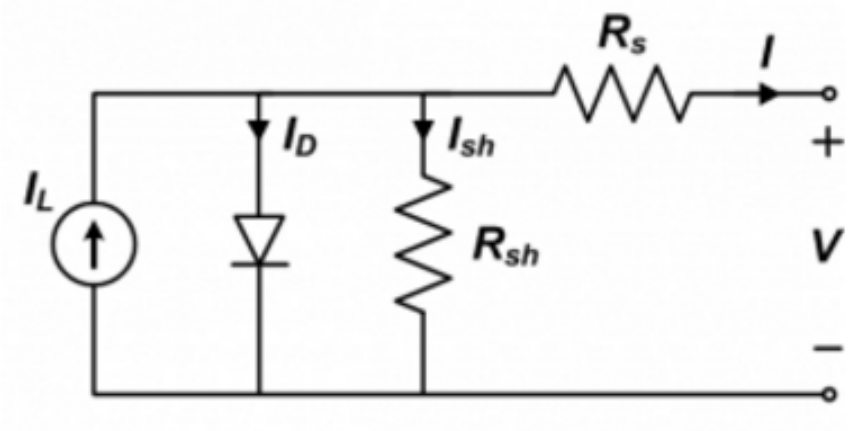

Figure A.1: Circuit model of a solar cell [14]

The circuit model contains: a current source arising from the absorbed light generating electrons and holes, a diode from the directional properties of the solar cell, a series resistor R_s, and a shunt resistance R_{sh}. The total current through the circuit can therefore be described as

$$I = I_L - I_D - I_{SH} \tag{A.1}$$

I is the output current of the solar cell, I_L is the photo-generated current, I_D is the diode current and I_{sh} is the current passing through the shunt resistance. Expanding this equation with the substitution of the diode current with the equation of current in a diode and the shunt current with the resistive loss yields, Thus, the equation for a single diode model is described as,

$$I = I_L - I_0 \left[\exp\left(\frac{V + IR_s}{nV_T} - 1\right)\right] - \frac{V + IR_s}{R_{sh}} \tag{A.2}$$

with I_0 is the diode reverse saturation current, n is the diode ideality factor, and V_T is the thermal voltage. [14]

A2 Current-Voltage Characteristic

The basic principle of electrical characterization measurement of a solar cell is its measured current density as a function of applied voltage bias (I-V) curve, shown in Fig. A.2. This curve is usually measured under two illumination conditions: no illumination and standard illumination. Standard

illumination is referred to as Air Mass 1.5 (AM 1.5) illumination, the standardized spectrum adopted by the community when measuring the efficiency of most solar cells [53]. Its intensity is standardized to 1000W/m^2.

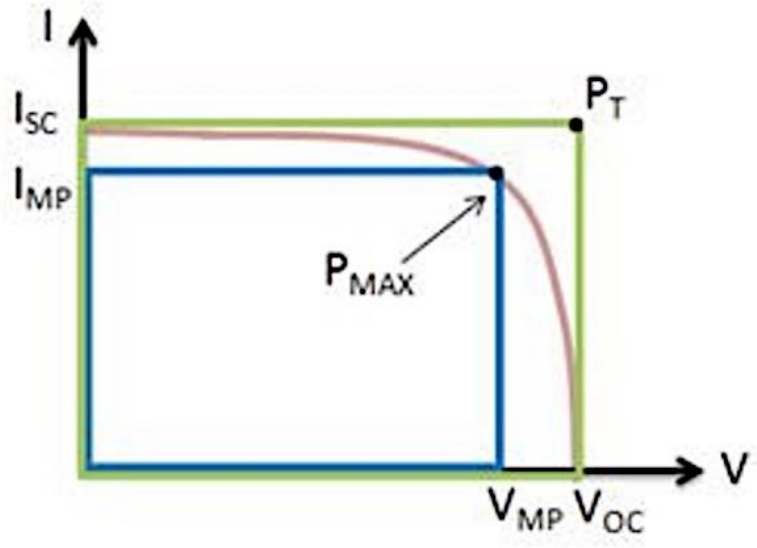

Figure A.2: Current-Voltage characteristic curve (red curve) [14]

From Fig A.2, three points of interest are highlighted on the red curve, which are: short-circuit current (I_{SC}), open-circuit voltage (V_{oc}), and the maximum output power (P_{max}). The V_{OC} is the maximum voltage the solar cell will produce for the load resistor, while the short-circuit current is the current through the solar cell when the voltage across the cell is zero (i.e. when the solar cell is short circuited). The blue curve represents the curve of the maximum power point, which includes current of maximum power point I_{MP} and voltage of maximum power point V_{OC}. The fill factor (FF) is defined as the relation between the areas of the blue curve to the area of the green curve. Equation A.3 defines the FF.

$$FF = \frac{P_{max}}{P_T} = \frac{I_{MP} \cdot V_{MP}}{I_{SC} \cdot V_{OC}} \tag{A.3}$$

As fill factor measures the degree of "squareness" of the characteristics, a solar cell with a higher voltage has a larger possible FF since the "rounded" portion of the IV curve takes up less area. Furthermore, this FF effects also the efficiency of the cell and is expressed as,

$$\eta = \frac{I_{SC} \cdot V_{OC} \cdot FF}{1000W/m^2} \tag{A.4}$$

where $I_{SC} \cdot V_{OC} \cdot FF$ is the maximum output power density and 100mW/cm^2 is the approximate incident illumination power density under AM 1.5 illumination condition. [14]

To measure the I-V curve, ECN uses the Neonsee machine that includes light source, measurement electronics, computer and software needed to measure solar cell I-V curves. The solar simulator is

able to measuring the solar cell's performance by performing a IV sweep and it is done by scanning an applied voltage across the solar cell and measure the current response of the cell.

A3 Quantum Efficiency

The quantum efficiency (QE) of a cell is the ratio of the number of collected electrons to the number of photons incident to the device as a function of photon energy [15]. The principle of external quantum efficiency (EQE) measurement is based on illuminating the sample by a monochromatic light and recording the device electrical current (number of generated carriers). By varying the frequency of the light, the entire curve of the current as a function of wavelength can be established. The area under the curve will then represent the total number of carriers created by the device under full spectrum white light illumination. In other words, the integration of the curve will give the electrical current density. The ideal EQE curve has a square shape, with a unity value for all wavelengths. In a real solar cell, however, the shape is dependent on both optical and electrical losses. An example, for crystalline silicon EQE graph is shown in Fig. A.3.

$$QE(\lambda) = \frac{no.of\ collected\ electrons}{no.of\ incident\ photons\ (\lambda)} \tag{A.5}$$

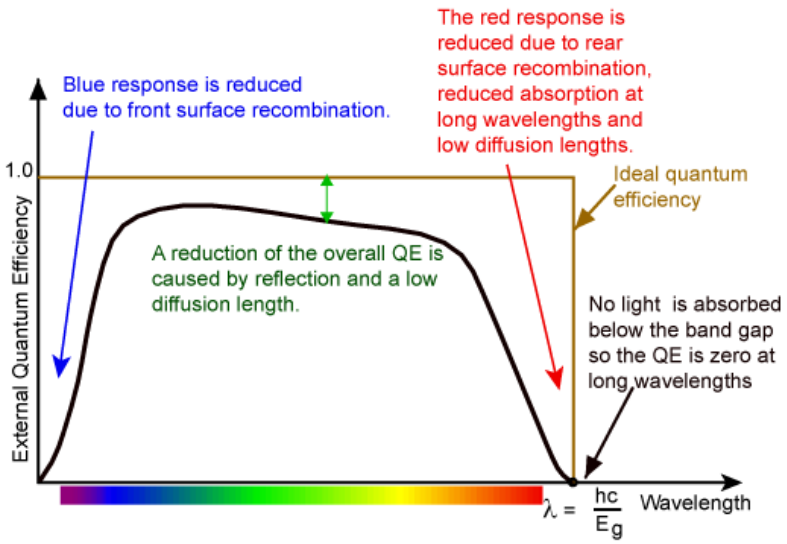

Figure A.3: Typical EQE measurement of a silicon cell with a band gap of 0.8 [15]

If all photons of a certain wavelength are absorbed and the resulting minority carriers are collected, then the QE at that particular wavelength is unity. The QE for photons with energy below the band gap is zero. In the case of an ideal cell, QE has the square shape shown above, however, the QE for most solar cells is reduced because of recombination effects. The same mechanisms which affect the collection probability also affect the QE. For example, front surface passivation affects carriers generated near the surface, and since blue light is absorbed very close to the surface, high front surface recombination will affect the "blue" portion of the quantum efficiency. Similarly, green light is absorbed in the bulk of a solar cell and a low diffusion length will affect the collection probability from

the solar cell bulk and reduce the quantum efficiency in the green portion of the spectrum. The QE can be viewed as the collection probability due the generation profile of a single wavelength, integrated over the device thickness and normalized to the incident number of photons.

A cell's short circuit current density can be calculated by integrating a cell's QE response weighted by the AM 1.5 solar spectrum, expressed in photon-flux units as [53],

$$J_{SC} = q \int_0^{\infty} QE(\lambda) AM1.5(\lambda) d\lambda \tag{A.6}$$

A4 Spectral Response Photoluminescence

PL spectroscopy is a powerful method to study electronic structure of semiconductors. It can determine the band gap, which is the fundamental energy scale in semiconductors [54]. In practice, the technique consists of absorbing photons at energies higher than its band gap, thus, creating electron-hole pair that will emit back photons from recombining, which is called PL. This PL can be spectrally resolved to get the required information about the energy levels. Experimentally, a laser is used to photo-excite electrons in a semiconductor and when they spontaneously de-excite, they emit luminescence. The luminescence is analyzed with a spectrometer and the peaks in the spectra represent a direct measure of the energy levels in the semiconductor [55].

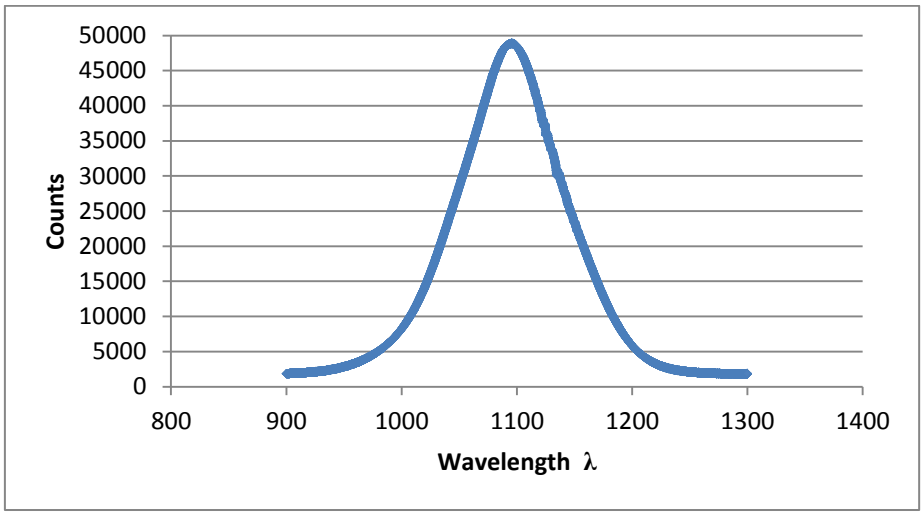

Figure 3.5: PL spectra of a CIGS

From the PL spectra seen in Fig. 3.5, we can determine the band gap by using *Planck's equation*,

$$E_g = \frac{hc}{\lambda} \tag{A.7}$$

with c as in speed of light (3×10^8 m/s), h as Planck's constant (4.13×10^{-15} eVs), and λ of the peak of PL spectra. In this case, the band gap is 1.13eV, with a λ of 1096nm.

A5 Reciprocity Theorem

The paper in Ref [56] gives a detailed theory of the reciprocity theorem, relating the carrier collection properties of a solar cell to its spectral EL emission. The theorem approaches the Shockley-Queisser identity of an LED and a solar cell in the limit of infinite charge carrier mobility μ_p and of an infinite non-radiative lifetime τ_{nr}.

The thermal equilibrium between a cell and its surroundings (such as the ambient in the dark) brings the well-known detailed balance principle where the emissivity of the cell $\epsilon(\omega)$ is equal to the absorptivity $a(\omega)$ [57]. Moreover, a reciprocity relation has been demonstrated by Donolato [58] describing the carriers transport within the cell. A more general law has therefore been derived between the luminescence emitted from a LED and the EQE of a solar cell. This relation can be seen as a generalized detailed balance principle taking into account the electronic transport. The emitted photon flux is described in Eq. 3,

$$\Phi_{el}(E) = Q_e(E)\Phi_{bb}(E)[exp(\frac{qVi}{kT}) - 1] \quad \text{(A.8)}$$